Early changes in the properties of CA3 engram cells explored with a novel viral tool

Dario Cupolillo[1,2], Noëlle Grosjean[1], Catherine Marneffe[1], Julio Viotti[1], Célia Reynaud[1], Séverine Deforges[1], Mario Carta[1], and Christophe Mulle[1*]

[1]Interdisciplinary Institute for Neuroscience, CNRS UMR 5297, University of Bordeaux, F-33000 Bordeaux, France

[2] current address: Italian Institute of Technology, Synaptic Plasticity of Inhibitory Networks, Genova, Italy

[*]Lead contact; correspondence: christophe.mulle@u-bordeaux.fr

Abstract

Forming new memories after a one-time experience requires initial encoding then consolidation over time. During learning, multimodal information converges onto the hippocampus, activating sparse neuronal assemblies which are thought to form a memory representation through concerted activity and synaptic interconnectivity. In this work, we use a novel tool for fast **fluorescent** labeling of engram neurons (FLEN). FLEN is based on c-Fos activity-dependent transient expression of a destabilized fluorescent marker ZsGreen1 rapidly after one-trial learning. With FLEN, we explore the electrophysiological properties of c-Fos activated CA3 pyramidal neurons a few hours following one-trial learning of an episodic-like memory. In parallel, we employ the Robust Activity Marker (RAM) system, which provides activity-dependent labelling 24 hours following a novel experience. Comparing FLEN+ and RAM+ neurons allows to characterize how the properties of neuronal assemblies evolve during an initial phase of consolidation. Whereas no difference was observed in the excitability of FLEN+ vs. FLEN- neurons, RAM+ neurons were more excitable than RAM- neurons. This suggests that CA3 pyramidal neurons recruited in an engram progressively acquire increased excitability as compared to neurons which were not activated by the one-trial contextual memory task. On the other hand, like RAM+ neurons, FLEN+ CA3 neurons show an increased number of excitatory inputs. Overall, with the FLEN strategy, we can show that both the intrinsic excitability and the synaptic properties of CA3 pyramidal neurons undergo progressive plastic changes over the first day following a one-trial memory task.

Introduction

Animal survival depends on the ability to rapidly form new and durable episodic memories of one-time meaningful events which, when recalled, allow to adapt behavior (Tulving, 2002). Contextual memories of ongoing experiences are continuously and rapidly generated in the hippocampus and subsequently stored in an extended cortical network (Eichenbaum, 2000). Computational models of memory point to a crucial role of the hippocampal CA3 region in episodic memory encoding and retrieval (Kesner & Rolls, 2015). Based on its distinctive extensive recurrent architecture (CA3-CA3), CA3 may act as an auto-associative or attractor network, enabling pattern completion during recollection (Kesner & Rolls, 2015; McNaughton, 1987). Indeed, mice with CA3-specific synaptic plasticity impairment (CA3 NR1-KO mice) are unable to encode the novel location of a hidden platform in a delayed matching-to-place version of the Morris water maze (K. Nakazawa et al., 2003) and to retrieve the learned position of a submerged platform when partial cues are presented (K. Nakazawa et al., 2002). In addition to recurrent connections, the main excitatory synaptic drivers of CA3 pyramidal neurons (PNs) are inputs from medial and lateral entorhinal cortex (MEC and LEC) via the perforant pathway (PP), and indirectly from mossy fibers (Mfs) through the dentate gyrus (DG). Mf inputs display 'conditional detonator' properties, enabling individual Mf synapses to trigger postsynaptic firing in response to repetitive firing of presynaptic DG cells (Henze et al., 2002; Marneffe et al., 2024; Rebola et al., 2017; Sachidhanandam et al., 2009; Vandael & Jonas, 2024).

During encoding of novel information, the orchestrated activity patterns of selected neuronal groups distributed throughout the brain, called engrams, represent the initial memory trace (Josselyn & Tonegawa, 2020). Engrams undergo long-lasting synaptic modifications during consolidation and are selectively re-engaged when the memory is retrieved (Bessières et al., 2024; Goto et al., 2021; Josselyn & Tonegawa, 2020; Kitamura et al., 2017; Ryan et al., 2015; Tomé et al., 2024). Experimental manipulation of neuronal engrams in the hippocampus allows selective memory erasure (Han et al., 2009), artificial memory recall (Liu et al., 2012) and creation of a synthetic memory (Vetere et al., 2019), highlighting both their necessity and sufficiency for memory functions.

The investigation of the properties of engram neurons has taken advantage of immediate early genes (IEGs) such as c-Fos, Arc (activity-regulated cytoskeleton-associated protein), or *Npas4* (neuronal PAS domain protein 4) to visualize and label neurons active during a memory task (DeNardo et al., 2019; Kawashima et al., 2013; Reijmers et al., 2007; Sørensen et al., 2016; X. Sun et al., 2020). Generally, IEGs are rapidly and transiently expressed; however different IEGs are triggered by different sets of

58 extracellular events and possess specific expression kinetics. Temporal control of IEG-based systems is
59 crucial to accurately link engram labeling to specific events that occur in a specific in time.

60 The activity of engram neurons can be tracked *in vivo* during their maturation from the process of
61 encoding throughout consolidation in behaving mice, by means of functional indicators like GCaMP
62 (Milczarek et al., 2018; Mocle et al., 2024; Tomé et al., 2024). However, *in vivo* Ca^{2+} imaging does not
63 allow to address the synaptic and intrinsic properties of engram neurons. Labeling of engram neurons in
64 order to characterize these properties *ex vivo* over time after an experience has occurred, often relies
65 on labeling techniques using inducible transgenic systems (DeNardo et al., 2019; Reijmers et al., 2007).
66 In several studies using transgenic mouse lines, engram labeling requires 48 hours of doxycycline (Dox)
67 deprivation before a novel experience (Kitamura et al., 2017; Liu et al., 2012; Pignatelli et al., 2019; Ryan
68 et al., 2015), or the use of tamoxifen injection to open a 12-hour time window for engram labeling
69 (DeNardo et al., 2019). Therefore, these systems only offer temporal control over extended time
70 windows, thus increasing the probability of compromising the experience specificity of labeled engram
71 cells. In addition, most of these approaches drive a relatively late labeling, enabling investigation of
72 learning-induced modifications more than 24 hours after a novel experience (e.g. RAM system) (X. Sun
73 et al., 2020) or shortly after recall for neurons which have been labeled several days before (Pignatelli et
74 al., 2019), when consolidation processes have already been engaged.

75 Little has been learned about how neuronal engrams in the hippocampus rapidly (in the time range of
76 hours) adapt their synaptic and physiological properties following encoding of a memory event, and how
77 these properties evolve over time. In this sense, it is unknown whether initial memory storage is
78 enabled by engram cell modifications of intrinsic properties, synaptic plasticity or a combination of
79 them. Here, we tackle these questions using a combination of viral strategies that allow us to identify
80 engram neurons and compare *ex vivo* their properties shortly after learning (3-4 hours), and 24 hours
81 after the experience has occurred (Fig. 1A)(Cupolillo, 2021). To track early engrams, we developed a
82 virally delivered c-Fos-based genetic construct that provides physiological-like rapid expression and fast-
83 decay of the bright fluorescent cytosolic marker ZsGreen1. This novel viral strategy for fast and efficient
84 labeling of engram neurons (FLEN) allows to identify and characterize engram neurons within 3-4 hours
85 following a novel experience, in reference to non-activated neurons. Then, to understand how initial
86 engram cell properties evolve within a 24-hour time scale, we employ the more durable c-Fos-based
87 artificial RAM system (Sørensen et al., 2016) to label neurons and characterize their properties 24 hours
88 after the exposure to a one-trial memory task.

Results

Creation and validation of c-Fos-ZsGreen1-DR for fast-labeling of engram neurons (FLEN).

We generated a genetic cassette for adeno-associated virus-mediated delivery which allows fast labelling of engram neurons (FLEN). This construct includes the full-length, activity-dependent c-Fos promoter which controls the expression of a destabilized variant of the green fluorescent protein ZsGreen1 (Matz et al., 1999) (Fig. 1B). The complete sequence of the c-Fos promoter ensures a physiological-like gene expression of ZsGreen1, which follows c-Fos expression. ZsGreen1 provides a bright whole-cell somatic and dendritic labelling of activated neurons (Fig. 1B). To restrict the labelling time window and minimize labeling unrelated to the designed experience, ZsGreen1 was fused with a destabilizing domain (DR); when fused to EGFP, DR decreases the fluorescence half-time to 2 hours (Li et al., 1998).

To determine the expression kinetics of FLEN in response to neuronal activity, P0 mouse cortical neurons were cultured (cellular density $3x10^5$ cells/well) and then co-infected at DIV3 with AAV9-c-Fos/ZsGreen1-DR (FLEN) and a secondary AAV9-CB7/mCherry, which constitutively expresses mCherry in infected neurons (Fig. 1B-C). Neurons were cultured until DIV11 in regular neurobasal medium, before switching to an activating medium containing 4-aminopyridine (4-AP, 100 µM) and bicuculline (Bic, 10 µM) for 30 minutes. The drugs were then washed out, and tetrodotoxin (TTX, 0.5 µM) was added to block further neuronal activity until cells were fixed (Fig. 1C). The percentage of activated neurons (ZsGreen+, further named FLEN+ neurons) over the total number of transduced neurons (mCherry+ neurons) was calculated at different time points within a 6-hour period after pharmacological stimulation. Only a limited number of FLEN+ neurons could be found in unstimulated conditions (5.4 ± 0.5 FLEN+/FLEN-, n=3 plates) (Fig. 1D-E). The activating medium triggered ZsGreen1 expression in neurons as early as 2 hours, reaching a 3-fold peak within 3 hours (1 hour: 6.7 ± 1.0, n=3; 2 hours: 13.2 ± 5.0, n=3; 3 hours: 15.7 ± 2.2, n=5) (Fig. 1D-E). The number of FLEN+ neurons decreased after the peak, decaying to pre-stimulation-like levels within 6 hours (4.5 hours: 12.0 ± 3.9, n=4; 6 hours: 5.0 ± 1.1, n=4) (Fig. 1D-E). Thus, FLEN showed a rapid induction (2-3 hours) and a fast decay (within 6 hours) of ZsGreen1-DR fluorescence (one-way ANOVA, p=0.04). To test specificity, we assessed co-expression with endogenous c-Fos in hippocampal cultures 3 hours following the same pharmacological stimulation. Among infected neurons (mCherry+), we found that 77.1 ± 6.3 % (n=4) of FLEN+neurons were positive for c-Fos. We also found that 60.8 ± 5.4 % (n=4) of the c-Fos-+neurons were also positive for FLEN. Thus,

119 although FLEN does not capture the entire c-Fos+ population, FLEN+ neurons are likely true engram (c-
120 Fos+) cells.

121 **FLEN captures early neuronal activity following CFC**

122 We next investigated the time course of FLEN expression *in vivo* in wild-type mice in response to
123 exposure to a salient novel experience. We virally targeted bilaterally dorsal CA3 in adult mice (2–3-
124 month-old) co-injecting AAV9-c-Fos/ZsGreen1-DR and the infection control AAV9-CB7/mCherry (Fig. 2A).
125 Then, mice were subjected to contextual fear conditioning (CFC), a hippocampal-dependent one-trial
126 memory task. During this task, mice learned to associate the delivery of 3 mild foot-shocks (0.4 pA, 2
127 seconds) with a specific environment (Fig. 2B). We found that CFC, a one-trial experience, can generate
128 a strong context-specific fear memory, as mice responded by freezing when re-exposed to the
129 conditioning environment 1 hour after training (HC: 14.7% ± 2.3%, 1-hour post-CFC: 47.4% ± 7.9%, n=7,
130 unpaired t-test, p=0. 0018), a response that outlasted 24 hours after training, but was not triggered in an
131 unfamiliar novel environment, nor when they were left undisturbed in their home cage (HC) (HC: 18.7%
132 ± 3.5%, 24 hours post-CFC: 61.5% ± 7.5%, neutral: 14.3% ± 4.5%, n=8, one-way ANOVA, Tukey's post-hoc
133 test HC : 1 hour post-CFC p =0.00004, HC : Neutral p=0 .84116, Neutral :1 hour post-CFC p=0.00001) (Fig.
134 2B).

135 The percentage of FLEN+ CA3 neurons (i. e. that display FLEN+/mCherry+ labeling, Fig. 2C) among the
136 overall population of infected neurons (FLEN-, i. e. that display mCherry+ labeling) was quantified 1.5, 3,
137 4.5, 6 and 12 hours following CFC and compared to that of untrained mice . Consistent with previous
138 studies (Sørensen et al., 2016; Weng et al., 2018), less than 2% of infected CA3 neurons were reported
139 to be labeled in the absence of a novel experience (Fig. 2D-E, HC, 0.84% ± 0.29% FLEN+/mCherry+, n=6).
140 One-trial CFC conditioning generated an engram, as indicated by an increase in FLEN+ neurons in CA3 in
141 the following hours (Fig 2D-E). Specifically, CA3 displayed 1.11% ± 0.42% FLEN+ neurons 1.5 hours after
142 CFC (n=5), which increased to 3.11% ± 0.74% 3 hours post-CFC (n=4) and 2.31 ± 0.44% at 4.5 hours post-
143 CFC (n=7). The fraction of active cells returned to basal-like levels at 6 hours (1.86 ± 0.16% FLEN+/
144 mCherry+, n=5) and further decreased 12 hours post-CFC (0.73% ± 0.32% FLEN+/ mCherry+, n=4) (Fig.
145 2D-E). Overall, the emergence of FLEN assembly peaks 3 hours following CFC and significantly decreases
146 12 hours later (one-way ANOVA p=0.003, *post hoc* Tukey's multiple comparisons test: HC vs. 3 h
147 p=0.008, 1.5 h vs. 3 h p=0.04, 3h vs. 12h p=0.01), faithfully mimicking the progression and transient
148 nature of native c-Fos expression (Holtmaat & Caroni, 2016).

149 We sought to probe CA3 engram formation 3 hours after different behavioral situations, namely
150 context-only (CO) and immediate-shock (IS) conditions, which offer the possibility for spatial exploration
151 only and no spatial exploration at all, respectively (Fig. S1A). In CO conditions, mice were allowed to
152 freely explore a novel cue-enriched arena. Comparably to other exploratory tasks, we found an increase
153 in the number of FLEN+ CA3 PNs 3 hours following CO (3.50 ± 1.18 % FLEN+/FLEN-, n=5) compared to
154 control HC mice (Kruskal-Wallis non-parametric test, p=0.03; Dunn *post hoc* multiple comparisons test,
155 p=0.02) (Fig. S2B). In the IS test, a 6-second-long foot-shock was delivered 2 seconds after the mouse
156 was placed in the conditioning cage, preventing sensorial sampling of the novel context (Fig. S1A). In
157 contrast, the IS test did not induce a significant increase in the number of FLEN+ in CA3 PNs as compared
158 to HC (1.84 ± 0.77 % FLEN+/FLEN-, n=4, Dunn *post hoc* multiple comparisons test, HC: IS, p=0.51) and to
159 context-only (CO: IS, p=0.88, n=4), possibly because of minimal spatial exploration.

160 Because of the reported functional heterogeneity of CA3 PNs in relation to memory encoding and recall,
161 which is directly related to their position within the proximodistal axis of CA3 (Nakamura et al., 2013; Y.
162 Nakazawa et al., 2016; Q. Sun et al., 2017), we analyzed the spatial distribution of FLEN+ PNs within CA3
163 pyramidal layer along the proximodistal and superficial-to-deep axis of CA3, following one-trial CFC (Fig.
164 2F and Fig. S2). We found a clear skewedness in the location of FLEN+ neurons along the proximodistal
165 axis toward CA3a at all time points following CFC and following CO compared to HC (Kolgomorov-
166 Smirnov test: HC vs. 1.5 h post-CFC, p<0.001; HC vs. 3 h post-CFC, p<0.001; HC vs. 4.5 h post-CFC,
167 p<0.001; HC vs. 6 h post-CFC, p<0.001: HC vs. 12 h post-CFC, p<0.001; HC vs. CO, p<0.001: HC vs. IS,
168 p<0.001) whilst they appeared to be more evenly distributed along the superficial-deep axis
169 (Kolgomorov-Smirnov test: HC vs. 1.5 h post-CFC, p=0.013: HC vs. 3 h post-CFC, p<0.001; HC vs. 4.5 h
170 post-CFC, p<0.001; HC vs. 6h post-CFC, p<0.001; HC vs. 12 h post-CFC, p=0.61; HC vs. CO, p<0.001: HC vs.
171 IS, p=0.02) (Fig. 2F and Fig. S2). Overall, these data indicate that the FLEN labeling strategy faithfully
172 identifies neurons activated during a one-trial exposure to a novel context and allows to characterize the
173 morpho-functional properties of CA3 engram neurons shortly (< 6 hours) following the experience.

174 In parallel, we confirmed that the RAM system (Sørensen et al., 2016) is a powerful tool to tag neurons
175 selectively activated by CFC in a temporally controlled manner (Fig. S3A) (Sørensen et al., 2016; Weng et
176 al., 2018). To identify RAM+ neurons, we stereotaxically injected AAV9-RAM/tTA::TRE/EGFP and AAV9-
177 CB7/mCherry to label dorsal CA3 in wild-type mice (Fig. S3A). Mice were fed with doxycycline pellets
178 starting one day before injection and then switched to a regular food diet for 48 hours before CFC (Fig.
179 S3A). As reported, we found that the number of RAM+ neurons was notably higher 24 hours after CFC

180 with respect to HC conditions (% RAM+ vs. mCherry+ neurons, HC: 1.13 ± 0.18 %, n=5; CFC: 3.54 ± 0.77
181 %, n=5; Welch's t-test p=0.03) (Fig. S3B-C), although not to the same extend as in previous reports
182 (Sørensen et al., 2016). The ratio of FLEN+ neurons 3 hours after CFC over HC (approximately 3:1)
183 closely resembles that of RAM+ neurons 24 hours after CFC (approximately 3:1)

184 **CA3 engram neurons evolve from low to higher firing frequency over 24 hours**

185 To understand if rapid memory acquisition and early consolidation is supported by specific changes in
186 electrophysiological intrinsic properties, we performed whole-cell patch-clamp recordings of CA3 PNs
187 (mainly in CA3b) in acute hippocampal slices of young adult mice injected with either FLEN or RAM,
188 respectively (Fig. 3A). AAV9-c-Fos/ZsGreen1-DR or AAV9-RAM-tTA::TRE-EGFP viral constructs were
189 injected bilaterally in dorsal CA3, together with AAV9-CB7-mCherry (Fig. 3A). After CFC, mice were
190 returned to their home cage for 3 hours (FLEN) or 24 hours (RAM), to yield peak expression of ZsGreen1-
191 DR or EGFP and then sacrificed to collect parasagittal slices (Fig. 3A). Activity-dependent FLEN+ neurons
192 remained detectable in acute slices, enabling specific targeting of engram CA3 PNs neurons for
193 approximately 4 to 5 hours after slicing. Engram neurons (FLEN+ or RAM+) were compared to their
194 respective neighboring non-engram neurons (FLEN- or RAM-) (Fig. 3A).

195 We first investigated the intrinsic physiological properties of FLEN+ and RAM+ CA3 PNs. Indeed, the
196 probability for a neuron to be recruited in a memory engram is thought to depend on its inherent
197 excitability level at the time of learning (see Josselyn & Tonegawa, 2020 for review). We assessed input
198 resistance (R_i) by injecting a series of hyper- and depolarizing current pulses with the membrane
199 potential held at -70 mV (Fig. 3B). R_i did not change significantly between FLEN+ and FLEN- neurons
200 (FLEN+: 253 ± 35 MΩ, n=19; FLEN-: 210 ± 19 MΩ, n=30; non-parametric Mann-Whitney U test, p-
201 value=0.57) and was similar to RAM+ and RAM- neurons which were also no different between them
202 (RAM+: 323.7 ± 14.1 MΩ, n=21; RAM-: 396.1 ± 15.2 MΩ, n=30, parametric t-test, p=0.68) (Fig.3B).
203 Further depolarizing steps of current were injected until an action potential (AP) was fired. AP properties
204 such as threshold, amplitude, width, upstroke and downstroke were not statistically different between
205 FLEN+ and FLEN- neurons and between RAM+ and RAM- neurons (Fig. S4B, C; Table 1). To study the AP
206 firing pattern, we injected 1 s-long pulses of current just above rheobase (200 pA) (Fig. 3C). Overall, the
207 firing frequency was not different in the FLEN groups (FLEN+: 2.64 ± 0.65 Hz, FLEN-: 3.59 ±0.62 Hz,
208 Mann-Whitney U test, p=0.51) (Fig. 3C). More than half of the total number of APs occurred within the
209 first 100 ms for all CA3 PNs, showing a consistent discharge pattern across both FLEN+ and FLEN- cells
210 (Kolmogorov-Smirnov test, p-value=1.0) (Fig. 3D). In contrast to FLEN+ CA3 PNs, RAM+ CA3 PNs showed

211 a prolonged spiking activity which outlasted the first 100 ms (Fig. 3D).. Altogether, these results show
212 that early after encoding, FLEN+ CA3 PNs do not show differences in excitability or patterns of activity as
213 compared to control neurons. However, after 24 hours, CA3 engram cells display an increase in
214 excitability without changes in R_i.

215 **Synaptic properties of FLEN+ neurons**

216 To assess overall excitatory synaptic strength and overall number of active synaptic connections, we
217 recorded spontaneous excitatory post-synaptic currents (sEPSCs) in FLEN+ CA3 PNs while blocking
218 $GABA_A$-dependent inhibitory currents (Bicuculline, 10 µM). The average amplitude of sEPSCs was not
219 different between FLEN+ and FLEN- CA3 PNs (FLEN+: 29.7 ± 5.3 pA, n=10, FLEN-: 32.2 ± 3.7 pA, n=10,
220 Kolmogorov-Smirnov test, p = 0.99), whereas their frequency was increased (Inter-event interval (IEI),
221 FLEN+: 788 ± 152 ms, n=10, FLEN-: 930 ± 91 ms, n=10, Kolmogorov-Smirnov test, p < 0.005; frequency:
222 FLEN+: 1.64 ± 0.26 Hz, n=10, FLEN-: 1.19 ± 0.14 Hz, n=10, pair-wise Mann-Whitney U test, p = 0.27) (Fig.
223 4A). Similarly, 24 hours after a novel experience, the average amplitude of sEPSCs was similar between
224 RAM+ and RAM- CA3 PNs (RAM+: 26.22 ± 2.46 pA, n=14; RAM-: 21.31 ± 2.72 pA, n=14, Kolmogorov-
225 Smirnov test, p=0.99) (Fig. 4A), but their frequency was significantly increased in RAM+ CA3 PNs (IEI:
226 RAM+: 645 ± 88 ms, n=17; RAM -: 1342 ± 207 ms, n=17; Kolmogorov-Smirnov test, p < 0.05; frequency:
227 RAM+: 2.04 ± 0.26 Hz, n=17, RAM-: 0.93 ± 0.11 Hz n=14, pair-wise Mann-Whitney U test, p = 0.001) (Fig.
228 4A).

229 Then, to investigate excitatory synaptic strength and release probability independent of network
230 activity, we measured miniature EPSCs (mEPSCs) by further adding TTX (0.5 µM). The average amplitude
231 was similar between FLEN+ and FLEN- neurons (FLEN+: 20.5 ± 2.5 pA, n=9, FLEN-: 18.7 ± 1.6 pA, n=14,
232 Kolmogorov-Smirnov test, p = 0.99), whereas we observed a higher frequency of mEPSCs in FLEN+
233 neurons as compared to control neurons (IEI: FLEN+: 1228 ± 186 ms, n=9, FLEN-: 1722 ± 242 ms, n=14,
234 Kolmogorov-Smirnov test, p < 0.0005; frequency: FLEN+: 1.48 ± 0.66 Hz, n=9, FLEN-: 0.69 ± 0.07 Hz,
235 n=14, pair-wise Mann-Whitney U test, p = 0.29) (Fig. 4B). Comparably, we found a higher frequency of
236 mEPSCs in RAM+ neurons as compared to RAM- CA3 PNs (IEI: RAM+: 782 ± 91 ms, n=14; RAM-: 1244 ±
237 247 ms, n=13; Kolmogorov-Smirnov test, p<0.005; frequency: FLEN+: 1.60 ± 0.23 Hz, n=14, FLEN-: 1.12 ±
238 0.20 Hz, n=13, pair-wise Mann-Whitney U test, p = 0.08), with unchanged amplitude (RAM+: 29.6 ± 4.8
239 pA, n=14, RAM-: 24.7 ± 4.2 pA, n=13,Kolmogorov-Smirnov test, p=0.99) (Fig. 4B). Thus, neurons
240 recruited in an engram appear to show increased excitatory drive after a few hours that persist after 24
241 hours, which may be linked to a higher number of synaptic contacts.

242 Previous reports indicate that CA3 PNs activated during by contextual learning and identified 24 hours
243 later by RAM had strengthened mossy fiber inputs (Weng et al., 2018). The existence of mEPSCs with
244 larger amplitudes may be related to synaptic plasticity in a subset of synapses, or theoretically to an
245 increased participation of Mf-driven mEPSCs (Henze et al., 2002). We thus calculated the proportion
246 miniature excitatory events with an amplitude greater than 40 pA. During spontaneous activity
247 recording, we found no difference in the fraction of putative Mf-driven inputs between FLEN+ and FLEN-
248 PNs (FLEN+: 0.09 ± 0.03 %, n= 9; FLEN-: 0.06 ± 0.02%, n=14; Mann-Whitney U Test p=0.33) and between
249 RAM+ and RAM- PNs 24 hours after learning (RAM+: 0.25 ± 0.08 %, n= 14; RAM-: 0.18 ± 0.07 %, n=13;
250 Mann Whitney U test, p=0.42) (Fig. 4B, inset). This later finding contrasts with earlier finding (Weng et
251 al., 2018), which found a selective strengthening of Mf inputs onto the ensemble of CA3 neurons
252 >24hours after activation by CFC. At variance with our analysis, this later study uses a mGluR2/3 agonist,
253 LY354740, which inhibits evoked Mf-CA3 synaptic transmission (Kamiya & Ozawa, 1999).

254 Inhibitory neurons are important in controlling spike generation of CA3 PNs, shaping network activity
255 and participation in neuronal assembly formation (Holtmaat & Caroni, 2016). We therefore probed
256 miniature inhibitory post-synaptic currents (mIPSCs), comparing FLEN+ vs. FLEN- neurons and RAM+ vs.
257 RAM- neurons, in the presence of NBQX (20 µM), D-AP5 (50 µM) and TTX (0.5 µM). We found that
258 mIPSCs were statistically more frequent (IEI: FLEN+: 340.1 ± 4.0 ms, n=4, FLEN-: 511.0 ± 40.5 ms, n=14,
259 Kolmogorov-Smirnov test, p < 0.005; frequency: FLEN+: 3.06 ± 0.35 Hz, n=4, FLEN-: 2.09 ± 0.14 Hz, n=14,
260 pair-wise Student's T test, p = 0.008), but their amplitude was on average comparable in FLEN+ vs. FLEN-
261 neurons (FLEN+: 35.1 ± 2.3 pA, n=4, FLEN+: 31.7 ±2.2 pA, n=14, Kolmogorov-Smirnov test, p = 0.99,
262 Welch's t-test, p = 0.30) (Fig. 4C). At 24 hours after learning, RAM+ neurons showed an increase in the
263 frequency of mIPSC (IEI: 330.5 ± 51.9 ms, n=6; frequency: 3.48 ± 0.60 Hz, n=6) compared to RAM-
264 neurons (IEI: 437.1 ± 47.1 ms, n=11, Kolmogorov-Smirnov test, p < 0.005; frequency: 2.52 ± 0.23 Hz,
265 n=11, pair-wise Mann-Whitney U test, p = 0.09), but no difference in their amplitude (RAM+: 22.7 ±1. 8
266 pA, n=11; RAM-: 26.5 ± 5.2, n=6, Kolmogorov-Smirnov test, p=0.89) (Fig. 4C). The frequency of all
267 excitatory and inhibitory inputs was elevated after CFC, both after 3 hours and after 24 hours, but not
268 their amplitude.

269 **Mf-CA3 synapses and feedforward inhibition in FLEN+ neurons**

270 Mf-CA3 connections between the DG and CA3 pyramidal cells provide powerful inputs via 'giant' Mf
271 boutons to CA3 PCs, which are thought to assist CA3 in the encoding of memory (Marneffe et al., 2024;
272 Vandael & Jonas, 2024). We recorded EPSCs evoked by minimal stimulation of Mfs (Marchal & Mulle,

273 2004) in FLEN+ and FLEN- CA3 PNs using an extracellular electrode placed within the DG hilus to
274 stimulate the Mf axonal bundle (Fig. 5A). Low-frequency stimulation (0.1 Hz) evoked EPSCs of variable
275 amplitude that, on average, did not differ between FLEN+ (81.7 ± 17.5 pA) and FLEN- neurons (80.8 ±
276 13.5 pA, Welch's t-test p = 0.97) (Fig. 5B). Increasing stimulation frequency to 1 Hz induced short-term
277 presynaptic frequency facilitation, causing an approximatively 3-fold increase in evoked current
278 amplitude in both FLEN+ (258.3 ± 49.5 pA) and FLEN- neurons (238.2 ± 39.0 pA, Welch's t-test p = 0.76)
279 (Fig. 5B). The EPSC facilitation ratio (1Hz vs. 0.1 Hz) was not different between FLEN+ and FLEN- neurons
280 (FLEN+: 3.28 ± 0.40, FLEN-: 3.28 ± 0.57, Welch's t-test p = 0.99) (Fig. 5B).

281 One-trial memory tasks reversibly induce a robust and rapid (within hours) increase in the number of
282 filopodia emanating from Mf synaptic terminals which contact GABAergic interneurons (Ruediger et al.,
283 2011), lending support to the hypothesis of an increase in feedforward inhibition in most CA3 PNs.
284 Because of the rapid time course with which structural plasticity occurs at Mf-CA3 synapses following
285 one-trial memory task, we took advantage of FLEN to explore a functional counterpart to structural
286 plasticity, and to address whether the change in feedforward inhibition was differentially affected in
287 FLEN+ vs. FLEN- CA3 PNs. We recorded excitatory and inhibitory synaptic currents in CA3 PNs while
288 stimulating Mfs (Fig. 5A). To calculate the excitatory to inhibitory (E/I) ratio at these synapses, we first
289 recorded evoked EPSCs by holding cells at the experimentally determined $GABA_A$ reversal potential (E_{Cl1-}
290 =-70 mV), and then at the reversal potential for cations (E_{Na1+} = +5 mV) (Fig. 5C) (Torborg et al., 2010).
291 We measured the peak amplitude of evoked EPSCs and IPSCs at a stimulation rate of 0.1 Hz to prevent
292 frequency facilitation (Fig. 5C). We found that the EPSC/IPSC ratio was higher in FLEN+ vs FLEN- cells,
293 although this is not significantly different (FLEN+: 3.48 ± 0.96, FLEN-: 2.20 ± 0.42, Welch's t-test, p =
294 0.27) (Fig. 5C). These data do not support the notion that shortly after one-trial learning, there is an
295 increase in feedforward inhibition at Mf-CA3 synapses.

296 **Discussion**

297 In the past decade, the search for engrams and the characterization of engram cells has largely
298 benefited from new gene targeting approaches to label the cells and to control their reactivation
299 (Josselyn & Tonegawa, 2020). The primary goal of our work was to test the hypothesis that the
300 functional properties of hippocampal cells activated during a one-trial contextual memory task were
301 distinct from surrounding ones shortly (3-6 hours) after encoding and were subject to progressive plastic
302 changes which could be linked to a first phase of memory consolidation.

303 Most techniques currently employed to study the properties of engram cells *ex vivo*, combine promoter
304 expression based on IEGs, intersectional transgenic strategies, optogenetics and pharmacogenetics with
305 behavioral paradigms (Denny et al., 2014; Pignatelli et al., 2019; X. Sun et al., 2020; Tonegawa et al.,
306 2015). A major caveat for using activity-dependent promoter/enhancers is the background basal
307 expression which can result in the labeling of neurons unrelated to the triggering behavioral event. To
308 limit this, fluorescent marker and/or actuator expression can be temporally controlled by directly
309 coupling IEG promoters, such as c-Fos or synthetic promoters (RAM), to inducible systems such as the
310 doxycycline (Dox) or the tamoxifen (TAM) systems 7/16/2025 2:46:00 AMWith these approaches, the
311 physiological properties of engram vs. non-engram cells has been examined by *ex vivo* patch-clamp
312 recordings 24 hours to several days after the initial contextual memory task (Pignatelli et al., 2019;
313 Sørensen et al., 2016; Weng et al., 2018; Yap et al., 2021).

314 We thus developed a viral strategy for transient neuronal expression of a fluorescent protein (FLEN)
315 following the exposure of mice to a novel context making use of the full-length c-Fos promoter and of
316 the brightly fluorescent ZsGreen1 protein (8.6 times brighter that EGPF, (Bell et al., 2007)), engineered
317 to be quickly destabilized. The time course of expression of ZsGreen1 in FLEN labeled neurons peaked at
318 3 hours both after pharmacological activation in cultured neurons and *in vivo* after a 5-minute exposure
319 to a novel context. Neuron labeling persisted for a few hours, enabling *ex vivo* electrophysiological
320 characterization of neurons thought to be involved in the initial encoding of contextual memory. As with
321 all techniques based on IEG promoters, a small percentage of AAV-transduced neurons showed
322 ZsGreen1 fluorescence under control conditions (HC or no activation of cultured neurons). However,
323 following CFC, the number of FLEN labeled neurons increased by a factor of 3.12. The bright
324 fluorescence of ZsGreen1 enabled the electrophysiological characterization of FLEN+ neurons, the
325 majority of which (>60%) were activated in relation to the CFC memory task. Therefore, the key features
326 of the FLEN strategy as compared to other tools used to label engrams is that: (i) it uses an AAV-based
327 viral tool, (ii) a c-fos promoter drives the expression of a brightly fluorescent protein allowing for their
328 identification *ex vivo* for functional analysis, (iii) the fluorescent protein is rapidly destabilized, providing
329 the possibility to label neurons only a few hours after their activation by a behavioural task.

330 We have used FLEN to label neurons in CA3, which is involved in the rapid encoding of new spatial and
331 contextual information (Kesner and Rolls, 2015). One of the key features of CA3 is the presence of
332 recurrent excitatory connections which are subject to NMDA-dependent synaptic plasticity (Rebola et
333 al., 2017), and this appears essential for memory of a one-trial experience (K. Nakazawa et al., 2003). It

334 has been proposed that the excitability state of neurons may contribute to memory formation (Zhang &
335 Linden, 2003). We first examined whether FLEN+ neurons showed distinctive intrinsic excitability
336 properties. We observed no difference in the membrane potential, input resistance, threshold or
337 bursting activity between FLEN+ and FLEN- neurons in slices prepared 3 hours following CFC. This
338 suggests that the subpopulation of CA3 PNs engaged in a one-trial learning task are not initially more
339 excitable than the general population of neurons, hence are not predetermined by their excitability
340 state. Alternatively, engram neurons may be transiently more excitable, at the time of encoding, and
341 lose this property within a few hours. In apparent contrast with our finding that FLEN+ CA3 PNs did not
342 show increased excitability, a simple associative memory task, trace eye-blink conditioning, appears to
343 increase the excitability of a large fraction (more than half) of CA3 neurons starting at 1 hour and
344 decreasing after several days (Thompson et al., 1996). Beyond the difference in the task and in the
345 species, these contrasting results may be explained by an overall **increased neuronal activity** related to
346 the learning task (Cai et al., 2016; Moyer et al., 1996), however not specific to engram neurons. This
347 does not preclude however the possibility that relative neuronal excitability immediately before training
348 could contribute to the selection of neurons to an engram as proposed in the amygdala (Yiu et al., 2014)
349 and the hippocampus (Mocle et al., 2024). However, in our hands, a one-trial memory task does not per
350 se trigger a selective increase in the excitability of engram neurons 3 hours after CFC as compared to the
351 general population of CA3 neurons. In the DG, recall of a previously stored contextual memory (48 hours
352 before), hence reactivation of engram neurons, rapidly increased the excitability of these engram
353 neurons (within 1 hour) with respect to engram neurons which were not subject to reactivation in a
354 separate group of mice (Pignatelli et al., 2019). A learning-related task may however induce plasticity of
355 intrinsic excitability of engram neurons on a longer time scale. We thus compared the intrinsic
356 excitability of FLEN+ neurons to those labeled more than 24 hours after CFC by using the previously
357 described RAM (Sørensen et al., 2016). We found that RAM+ neurons showed prolonged spike firing in
358 response to a depolarizing pulse of current, hence decreased accommodation in comparison with non-
359 labeled neurons. Considering that the set of neurons labeled by these two strategies may be of the same
360 set, based on the expression of a fluorescent marker under the control of the c-Fos promoter, our data
361 strongly suggest that engram neurons in CA3 progressively increase excitability as compared to neurons
362 which were not activated by the one-trial contextual memory task. As a limitation point, it should
363 however be considered that both strategies may label distinct populations of neurons, due to the use of
364 different promoters to drive the expression of the fluorescent marker. However, both strategies
365 accurately label neurons that are, in large part, c-Fos positive and are involved in processing specific

366 context information (see Fig 4, Sorensen et al, 2016). The acquisition of increased excitability 24 hours
367 after one-trial memory encoding suggests that intrinsic excitability is a key feature of an early
368 consolidation of memory, which may even be strengthened upon reactivation of memory (Pignatelli et
369 al., 2019). It would be interesting to assess whether increased intrinsic excitability persists throughout
370 further consolidation of memory.

371 Increased neuronal activity in engram neurons at the time of encoding may result from more efficient or
372 more synchronous excitatory synaptic inputs to these neurons. Here we observed that FLEN+ neurons
373 (hence characterized >3 hours after initial encoding) showed an increased excitatory drive, which may
374 be explained by a higher number of synaptic contacts, although an increase in release probability cannot
375 be excluded. We cannot discriminate whether the increased number of synaptic inputs preexists to the
376 formation of the engram, or whether it is a plastic mechanism taking place shortly following the
377 contextual memory. The time course of appearance of additional synapses, by unmuting of silent
378 synapses following contextual memory acquisition, is compatible with experimentally induced functional
379 and structural synaptic plasticity (Holtmaat & Caroni, 2016). On the other hand, if FLEN+ neurons
380 showed higher synaptic inputs at the time of memory encoding, this would increase the chance that
381 these neurons show increased excitation (c-Fos activation) hence participate in the engram. The
382 amplitude of mEPSCs in FLEN+ neurons does not appear to increase on average in comparison with
383 FLEN- CA3 PNs. This finding may not favor the possibility that LTP-like synaptic plasticity occurs early
384 during the process of memory formation. In this event, NMDA-dependent forms of synaptic plasticity
385 are more likely to occur later on during the early phase of consolidation of the memory trace (Humeau
386 & Choquet, 2019). Interestingly, we observed a comparable increase in the frequency of sEPSCs and
387 mEPSCs in RAM+ CA3 neurons 24 hours after CFC, as previously reported (Weng et al., 2018), without
388 any change in the amplitude. Using a pharmacological agent which selectively inhibits Mf-CA3
389 transmission, it was hypothesized that the increased mEPSC frequency is mainly due to more active Mf-
390 CA3 synapses (Weng et al., 2018). However, if this was the case, we would also expect an increase in the
391 amplitude of mEPSCs as well as an increase in the fraction of mEPSCs larger than 45 pA. In addition, we
392 did not find evidence for an increase in Mf-CA3-evoked EPSCs (see below). Overall, our data indicate
393 that CA3 engram neurons characterized a few hours after the one-trial memory task show a higher level
394 of excitatory synaptic inputs, and this feature seems to extend to 24 hours. We found no evidence for
395 increased amplitude of EPSCs in FLEN+ or RAM+ CA3 PNs which could have been indicative of
396 postsynaptic plasticity through an increased number of synaptic AMPA receptors (Humeau & Choquet,

397 2019; Takeuchi et al., 2014). One reason may be that synaptic plasticity only occurs in a subset of
398 synaptic contacts, and the recording of mEPSCs is not **sensitive** enough to capture these modifications

399 Local inhibition controls the spiking of CA3 PNs, hence their capacity to be engaged in an active
400 ensemble of neurons at the time of contextual memory encoding. In CA1, there is a fine control of
401 inhibition upon novel environment exploration (Yap et al., 2021) or fear learning (Lovett-Barron et al.,
402 2014). We found an increase in the frequency of mIPSCs after CFC in engram CA3 neurons, both after 3
403 hours and after 24 hours. This suggests that the elevation of mEPSCs in the engram neurons is
404 counterbalanced by increased inhibition, although this would need to be generally tested in conditions
405 of hippocampal circuit activity *in vivo*. We have also provided information on the process of Mf-driven
406 feedforward inhibition in CA3 following one-trial memory encoding. Mf-CA3 synapses have been
407 proposed to play a major role in assisting CA3 in the encoding of memory (Kesner & Rolls, 2015). For
408 these reasons, it is important to directly characterize the properties of Mf-CA3 synapses impinging on
409 CA3 engram neurons. We observed no difference in the amplitude and short-term plasticity of Mf-CA3
410 EPSCs evoked in FLEN+ CA3 neurons vs. FLEN- neurons. It has been proposed that 24 hours after CFC,
411 the increased amplitude of mEPSCs in RAM+ neurons can be attributed to modifications of Mf-CA3
412 synapses (Weng et al., 2018), which may suggest progressive plasticity of these inputs. There is
413 abundant evidence that the structural properties of Mf-CA3 synapses are modified by experience
414 (Ruediger et al., 2011)(Galimberti et al., 2006; Maruo et al., 2016). Feedforward inhibition combines
415 with short-term plasticity of Mf-CA3 synapses to define the physiological conditions for efficient spike
416 transfer between the DG and CA3 (Marneffe et al., 2024; Vandael & Jonas, 2024; Zucca et al., 2017). CFC
417 induces a robust and global increase in the number of filopodia emanating from the giant Mf terminals,
418 which peaks between 1 and 5 hours after the one-trial memory task and is related to the precision of
419 memory and the size of engrams (Ruediger et al., 2011). Because filopodia contact GABAergic
420 interneurons, this structural plasticity has been proposed to increase feedforward inhibition, albeit this
421 has not yet been demonstrated. Here we compared the excitation/inhibition ratio of Mf-evoked
422 synaptic responses between FLEN+ and FLEN- neurons. We did not observe a significant increase of
423 feedforward inhibition onto CA3 engrams, as may be expected from an increased number of filopodia,
424 but we rather observed a tendency towards less feedforward inhibition. This leads us to speculate that
425 shortly following contextual memory formation, Mf-driven feedforward inhibition is increased in the
426 general population of neurons but not in Mf inputs onto engram neurons, thus allowing for a
427 comparatively stronger input from the DG to the engram neurons. It will be interesting to test whether

428 this increased signal to noise ratio is maintained 24 hours after contextual memory encoding, given that
429 the number of filopodia per Mf bouton has returned to basal level (Ruediger et al., 2011).

430 In conclusion, we used a viral tool allowing for the identification of neurons involved in a behavioral task
431 within 3 hours, as a complement to the transgenic mouse strategies and viral vectors which have been
432 used to assess changes in engram neuron properties in the time range of days. Although it is not
433 possible to fully assess the electrophysiological properties of engram neurons at the time of the
434 encoding, this work shows that the engram neurons are not different in their intrinsic membrane
435 properties shortly after encoding. This set of properties may however follow delayed (progressive)
436 plastic changes which are evident 24 hours after initial encoding. Overall, we propose that engram
437 neurons do not show higher excitability preexisting to the selection of neurons to the engram during the
438 memory encoding task. Hence the increased activation state of the FLEN+ neurons at the time of
439 encoding may rather relate to a higher number of active synaptic inputs providing more efficient
440 excitation. Interestingly, although more work is needed to confirm this tendency, increased excitation
441 may also be linked to decreased Mf-driven feedforward inhibition, thus favoring spike transfer from the
442 DG to CA3 at the time or shortly after memory encoding. The FLEN viral tool will be useful to assess how
443 the properties of neurons in brain regions are involved in the contextual memory encoding process,
444 including the entorhinal cortex and the DG.

445

446 **Materials and methods**

447 **Animals**

448 C57Bl6j female mice were obtained from Janvier and cared according to the regulations of the
449 University of Bordeaux/CNRS Animal Care and Use Committee. Animals were housed with their
450 littermates with ad libitum access to food and water. Cages were kept in a temperature-regulated room
451 on a 12 h light/dark cycle. Prior to any behavioral test, all mice were single housed for 4-5 days and then
452 handled for at least 3 consecutive days. Mice injected with the RAM system were kept on a doxycycline
453 diet (4 mg/Kg) starting 1 day before the viral injection.

454 **Viral vectors**

455 Adeno-associated virus (AAV) serotype 2/9 vectors containing our custom-made c-Fos-ZsGreen1-DR
456 (titer $4.00x10^{13}$) were generated in our lab. The c-Fos promoter was subcloned from the Addgene_11983
457 construct (Mus musculus, size: 466 pb, position -380/+86). The AAV2/9 vectors containing the RAM
458 system (titer $3.39x10^{13}$) were purchased from AddGene (ID 84469). Each vector was mixed with an
459 infection marker virus AAV2/9-CB7/mCherry (titer $1.50x10^{13}$) and diluted 1:10 for co-injection.

460 **Cell culture and pharmacological activation**

461 P0 mouse cortical neurons were plated (300000 cells/well) and allowed to grow on glia cells. Plates were
462 stored in an incubator (37° C) for the duration of the experiment. At DIV3 cells were infected with the
463 viral mix of c-Fos-ZsGreen1-DR and CB7-mCherry. At DIV14, neurons were switched to an activating
464 medium containing 4-AP (100 µM) and Bicuculline (10 µM) for 30 minutes at 37°C. Then this activating
465 medium was washed and tetrodotoxin was added (0.5 µM) to prevent action potential firing and stop
466 neuronal activation. Neurons were then fixed using 4% paraformaldehyde (PFA) in 0.1 mM PBS at the
467 different intervals following pharmacological activation. To calculate FLEN/c-Fos overlap, neurons were
468 fixed as described above 3 hours after tetrodotoxin was added to the medium.

469 **c-Fos immunofluorescence**

470 Fixed cells were incubated with 50 mM ammonium chloride (NH_4Cl) in PBS for 10 minutes under
471 constant shaking (1 mL/well), and washed three times with PBS (5 minutes each). Permeabilization was
472 performed with 0.2% Triton X-100 in PBS for 5 minutes under shaking (1 mL/well), followed by three PBS
473 washes (5 minutes each). Non-specific binding sites were blocked with 2% bovine serum albumin (BSA)
474 in PBS for 60 minutes under shaking (1 mL/well). Primary antibody incubation was performed at RT for

475 60 minutes under shaking using rat anti-c-Fos (Synaptic Systems, ref 226 017) diluted 1:1000 in 2% BSA
476 (160 µL/coverslip). Coverslips were washed three times with 2% BSA in PBS (5 minutes each) and
477 incubated again in 2% BSA for 60 minutes under shaking (1 mL/well). Secondary antibody (goat anti-rat
478 Alexa Fluor 647, Thermo Fisher Scientific, ref A21247) was applied at 1:500 dilution (160 µL/coverslip)
479 for 60 minutes at RT under shaking and protected from light. Coverslips were washed three times in PBS
480 (5 minutes each) and mounted using Fluoromount-G with DAPI (Southern Biotech).

481 **Cell counting**

482 Culture and ex vivo slice images were processed using custom code. Each fluorescence channel
483 (mCherry, ZsGreen, c-Fos, and DAPI) was normalized, Gaussian-filtered and manually thresholded.
484 Binary masks were generated and cleaned by removing small objects and segmented using watershed.
485 Masks were further filtered by area and shape (circularity, axis ratio, eccentricity, solidity). From these
486 counts, labeling ratios (between ZsGreen, mCherry, c-Fos and DAPI) were calculated.

487 **Stereotaxic injection**

488 2-month-old C57Bl6j mice were bilaterally injected with either AAV9-c-Fos-ZsGreen1-DR or the AAV9-
489 RAM virus mixed with the infection control virus AAV9-CB7-mCherry into dorsal hippocampus. Mice
490 were anesthetized with 4% isoflurane and placed in a stereotaxic apparatus, where they were kept
491 under 1.5-2% isoflurane anesthesia (0.8-1 L/min), and injected with buprenorphine (0.1 mg/kg) and
492 carprofene (5 mg/kg) to prevent post-surgery pain. The injection volume and flow rate (300 nl at 60
493 nl/min) were controlled with an injection micro-pump (World Precision Instruments). Injection
494 coordinates, using bregma as a reference point, were as follows: AP -1.78, ML ± 2.40, DV -2.35. This site
495 targets dorsal CA3b, but virus spreading resulted in the infection of CA3a, CA3b, CA3c, CA2 and in some
496 cases few granule neurons and hilar cells of the DG. Mice were carefully monitored for 4 days following
497 surgery, and behavioral manipulation started after a recovery period of approximately 2 weeks.

498 **Behavioral tests**

499 Once recovered, mice were single-housed to reduce uncontrolled experiences that could contaminate
500 the ensemble of CFC-related labelled engram cells. Then, mice were handled to habituate to the
501 experimenter for at least 3 consecutive days prior to CFC. Mice injected with the RAM virus were
502 deprived of doxycycline, switching to a regular diet, 48 hours before CFC training. On the one-trial
503 learning day, mice were transported in the experimental room and immediately placed in a novel

504 conditioning chamber enclosed in a sound-attenuating cabinet (Ugo Basile), enriched with visual cues,
505 and allowed to explore it for a total duration of 300s. After an initial exploration period, 3 mild foot-
506 shocks (2s, 0.7 mA) were delivered at a 150s, 210s, and 270s, leaving 30s for additional context sampling
507 at the end. Mice were recorded and freezing behavior was scored using ANY-Maze 6 software (Stoelting
508 Europe). Freezing was detected as the absence of movement apart from respiration, and freezing events
509 were scored when immobility lasted more than a threshold of 300ms. Mice were then returned to their
510 home cage. For context only (CO) exploration, mice were placed in a 50 cm x 50 cm custom-built open
511 field, where some objects were distributed. Mice were allowed to explore for 5 minutes before
512 returning to their home cage. The immediate shock test was carried out in the fear conditioning system.
513 Mice explored the conditioning chamber for only 2 seconds before receiving a 6-second-long foot-shock
514 and then returned to their home cage.

515 **Histology**

516 Mice were anesthetized with intraperitoneal administration of a ketamine/xylazine mix (100 mg/kg/10
517 mg/kg) at different time intervals following CFC (1.5 h, 3 h, 4.5 h, 6 h, 12 h for c-Fos-ZsGreen1-DR, 24 h
518 for RAM). Mice were then intracardially perfused with 0.9% NaCl solution followed by 4%
519 paraformaldehyde (PFA) in 0.1 mM PBS. Brains were removed and postfixed in 4% PFA overnight at 4°C.
520 Brains were transferred in sucrose 30% in 0.1 mM PBS at 4°C until they sank. Brains were cut on a
521 cryostat into 25 µm-thick coronal sections and collected in PBS with 0.3% Triton X-100. Slices were
522 immediately mounted on glass slides and covered in DAPI-based mounting medium. The number of
523 fluorescent neurons was assessed directly without amplification.

524 **Confocal microscope**

525 Confocal acquisitions were performed using a Leica SP8 White Light Laser 2 on an inverted stand (Leica
526 Microsystems, Mannheim, Germany) and with a x20 (NA 0.75) immersion objective. Images were
527 analyzed using ImageJ. At least 5 slices per animal were acquired. Imaging of neuronal cultures was
528 carried out as well using confocal Leica SP8 White Light Laser 2 (Leica Microsystems, Mannheim,
529 Germany) and with a x20 (NA 0.75) immersion objective. In all experiments, the settings (laser power,
530 gain, offset) were fixed between groups as well as the pixel size (120 nm).

531 ***Ex vivo* slice preparation**

532 Slices were prepared 3 hours or 24 hours following CFC for c-Fos-ZsGreen1-DR-injected mice and RAM-
533 injected mice respectively. To attempt to reduce stress-related unspecific c-Fos activation, mice were
534 anesthetized with a ketamine/xylazine mix (100 mg/kg/10 mg/kg; i.p.) and intracardially perfused with
535 an ice-cold oxygenated (95% O2 and 5% CO2) cutting solution containing (in mM): 87 NaCl, 2.5 KCl, 1.25
536 NaH2PO4, 25 NaHCO3, 25 glucose, 75 sucrose, 0.5 CaCl2, 7 MgCl2, pH 7.4, 315 mOsm/kg. Brains were
537 quickly dissected out and parasagittal slices from both hemispheres (300 µm thick) were cut on a
538 vibratome (Leica VT1200S, Germany) in the same oxygenated ice-cold cutting solution. Slices were then
539 incubated at 34°C in a resting chamber containing the same cutting solution for 20-30 minutes for
540 recovery. Slices were then transferred in a resting chamber filled with an oxygenated (95% O2 and 5%
541 CO2) artificial cerebrospinal fluid (aCSF) containing (mM): 125 NaCl, 2.5 KCl, 1.25 NaH2PO4, 26 NaHCO3,
542 1.3 MgCl2, 2.3 CaCl2, 10 glucose, pH 7.4, 300 mOsm/kg at room temperature for the rest of the day.

543 **Electrophysiology**

544 When transferred to a recording chamber, slices were continuously superfused with aCSF. CA3
545 pyramidal cells were identified with an infrared differential interference contrast (IR-DIC) microscope
546 with a water immersion 63X objective (N.A. 0.8). Neurons were then classified as engram neurons
547 (simultaneous expression of ZsGreen1-DR/mCherry or EGFP/mCherry when RAM was used) or non-
548 engram neuron (mCherry expression only) with a 2p microscope. Whole-cell recordings were made at
549 room temperature using borosilicate glass capillaries with resistances between 4-6 MΩ. For current
550 clamp recordings, the intracellular solution contained (in mM): 135 K-gluconate, 5 KCl, 2 NaCl, 10 Na2-
551 phosphocreatine, 0.1 EGTA, 10 HEPES, 5 Mg-ATP, 0.4 Na-GTP, pH 7.2 adjusted with KOH, 280-290
552 mOsm/Kg. For voltage clamp mode, the patch pipettes were filled with a solution containing (mM): 140
553 Cs-methanesulfonate, 2 MgCl2, 4 NaCl, 5 Na-phosphocreatine, 0.2 EGTA, 10 HEPES, 3 Na2-ATP, 0.3 GTP,
554 pH 7.2 adjusted with CsOH, 280-290 mOsm/Kg. To record inhibitory currents, a high-chloride
555 intracellular solution was used, containing (mM): 103 CsCl, 12 $CsCH_3O_3S$, 5 TEA-Cl, 10 HEPES, 4 Mg-ATP,
556 0.5 Na-GTP, 1 $MgCl_2$, pH adjusted to 7.2 with CsOH, 280-290 mOsm/Kg. No liquid-junction correction
557 was used. Neurons were held at –70 mV. Leak current and series resistance were monitored throughout
558 each experiment; neurons with a leak current >200 pA and a series resistance >25MΩ or if these
559 parameters changed more than 20% were excluded from analysis. All recordings were performed 5-10
560 min after opening the membrane. Input resistance was quantified by linearly fitting the voltage change
561 against injected current. Steps of hyper- and depolarizing current steps were injected to determine

action potential threshold and rheobase. Action potential firing pattern was determined by injecting 200 pA steps of current. Spontaneous EPSCs (sEPSCs) were isolated by bath application of bicuculline (10 µM), while mEPSCs were recorded in presence of bicuculline (10 µM) and tetrodotoxin (0.5 µM). Spontaneous IPSCs (sIPSCs) were recorded in presence of D-AP5 (50 µM) and NBQX (20 µM), while mIPSCs were isolated in presence of D-AP5 (50 µM), NBQX (20 µM) and TTX (0.5 µM). Spontaneous and miniature synaptic events were detected using a deconvolution-based approach (Pernía-Andrade et al., 2012). To record evoked EPSCs (eEPSCs), stimulating glass pipettes (World Precision Instruments) were filled with aCSF and placed in the hilus, close to the granule cell layer to stimulate initial portion of Mf axons. Voltage pulses (200 µs) were delivered through a stimulus isolator (Digitimer, UK). Stimulation intensity was adjusted to obtain minimal Mf stimulation (Marchal and Mulle., 2004). Basal synaptic transmission was recorded while holding CA3 neurons at -70 mV with pulses delivered at a low frequency of 0.1 Hz. Frequency was then increased to 1 Hz to induce frequency facilitation. After 2-3 minutes, when facilitation was extinguished, the voltage was switched to +5 mV (reversal potential for cations) to record di-synaptic eIPSC. All recordings were obtained with a HEKA EPC10 amplifier, filtered at 3.3 kHz and digitized at 10 kHz via PatchMaster software (Lambrecht, Germany). Data was analyzed offline using custom-made Python scripts.

Statistical analysis and graphical representations

Statistical analyses and graphical representation were performed with custom-written Python codes using standard libraries (e.g. Numpy, Scipy, Pandas, Skimage). Data are presented as boxplots and scatter plots indicating the number of samples per group. Boxplots indicate median, first and third quartiles and whiskers represent the rest of the distribution. Bold horizontal and vertical lines on scattered data points represent mean and SEM respectively. Values were first tested for normality (D'Agostino and Pearson omnibus test or Shapiro-Wilk test). Normally distributed data were compared using a t-test (two-sided) while Mann–Whitney rank test (two-sided) was used for non-normal data set. Multiple group comparison was carried out using one-way ANOVA when data were normally distributed or Kruskalis-Wallis when normality did not apply. Tukey's *post hoc* comparison analysis or Dunn *post hoc* comparison analysis was applied. Cumulative frequency distributions and normalized distributions were tested using Kolgomorov-Smirnov test. Statistical differences were considered as significant at $p < 0.05$.

591 **References**

592 Bessières, B., Dupuis, J., Groc, L., Bontempi, B., & Nicole, O. (2024). Synaptic rearrangement of NMDA
593 receptors controls memory engram formation and malleability in the cortex. *Science Advances*, *10*(35).
594 https://doi.org/10.1126/sciadv.ado1148

595 Cupolillo, D. (2021). *Comparing properties of CA3 engram neurons over initial periods of encoding and*
596 *early phase of consolidation*. PhD, Université de Bordeaux. https://theses.hal.science/tel-03336166v1

597 DeNardo, L. A., Liu, C. D., Allen, W. E., Adams, E. L., Friedmann, D., Fu, L., Guenthner, C. J., Tessier-
598 Lavigne, M., & Luo, L. (2019). Temporal evolution of cortical ensembles promoting remote memory
599 retrieval. *Nature Neuroscience*, *22*(3), 460- 469. https://doi.org/10.1038/s41593-018-0318-7

600 Denny, C. A., Kheirbek, M. A., Alba, E. L., Tanaka, K. F., Brachman, R. A., Laughman, K. B., Tomm, N. K.,
601 Turi, G. F., Losonczy, A., & Hen, R. (2014). Hippocampal Memory Traces Are Differentially Modulated by
602 Experience, Time, and Adult Neurogenesis. *Neuron*, *83*(1), 189- 201.
603 https://doi.org/10.1016/j.neuron.2014.05.018

604 Eichenbaum, H. (2000). A cortical–hippocampal system for declarative memory. *Nature Reviews*
605 *Neuroscience*, *1*(1), 41- 50. https://doi.org/10.1038/35036213

606 Galimberti, I., Gogolla, N., Alberi, S., Santos, A. F., Muller, D., & Caroni, P. (2006). Long-Term
607 Rearrangements of Hippocampal Mossy Fiber Terminal Connectivity in the Adult Regulated by
608 Experience. *Neuron*, *50*(5), 749- 763. https://doi.org/10.1016/j.neuron.2006.04.026

609 Goto, A., Bota, A., Miya, K., Wang, J., Tsukamoto, S., Jiang, X., Hirai, D., Murayama, M., Matsuda, T.,
610 McHugh, T. J., Nagai, T., & Hayashi, Y. (2021). Stepwise synaptic plasticity events drive the early phase of
611 memory consolidation. *Science*, *374*(6569), 857- 863. https://doi.org/10.1126/science.abj9195

612 Han, J.-H., Kushner, S. A., Yiu, A. P., Hsiang, H.-L. (Liz), Buch, T., Waisman, A., Bontempi, B., Neve, R. L.,
613 Frankland, P. W., & Josselyn, S. A. (2009). Selective Erasure of a Fear Memory. *Science*, *323*(5920),
614 1492- 1496. https://doi.org/10.1126/science.1164139

615 Henze, D. A., Wittner, L., & Buzsáki, G. (2002). Single granule cells reliably discharge targets in the
616 hippocampal CA3 network in vivo. *Nature Neuroscience*, *5*(8), 790- 795. https://doi.org/10.1038/nn887

617 Holtmaat, A., & Caroni, P. (2016). Functional and structural underpinnings of neuronal assembly
618 formation in learning. *Nature Neuroscience*, *19*(12), 1553- 1562. https://doi.org/10.1038/nn.4418

619 Humeau, Y., & Choquet, D. (2019). The next generation of approaches to investigate the link between
620 synaptic plasticity and learning. *Nature Neuroscience*, *22*(10), 1536- 1543.
621 https://doi.org/10.1038/s41593-019-0480-6

622 Josselyn, S. A., & Tonegawa, S. (2020). Memory engrams : Recalling the past and imagining the future.
623 *Science*, *367*(6473), eaaw4325. https://doi.org/10.1126/science.aaw4325

624 Kamiya, H., & Ozawa, S. (1999). Dual mechanism for presynaptic modulation by axonal metabotropic
625 glutamate receptor at the mouse mossy fibre-CA3 synapse. *The Journal of Physiology*, *518*(2), 497- 506.
626 https://doi.org/10.1111/j.1469-7793.1999.0497p.x

Kawashima, T., Kitamura, K., Suzuki, K., Nonaka, M., Kamijo, S., Takemoto-Kimura, S., Kano, M., Okuno, H., Ohki, K., & Bito, H. (2013). Functional labeling of neurons and their projections using the synthetic activity–dependent promoter E-SARE. *Nature Methods*, *10*(9), 889-895. https://doi.org/10.1038/nmeth.2559

Kesner, R. P., & Rolls, E. T. (2015). A computational theory of hippocampal function, and tests of the theory : New developments. *Neuroscience & Biobehavioral Reviews*, *48*, 92-147. https://doi.org/10.1016/j.neubiorev.2014.11.009

Kitamura, T., Ogawa, S. K., Roy, D. S., Okuyama, T., Morrissey, M. D., Smith, L. M., Redondo, R. L., & Tonegawa, S. (2017). Engrams and circuits crucial for systems consolidation of a memory. *Science*, *356*(6333), 73-78. https://doi.org/10.1126/science.aam6808

Li, X., Zhao, X., Fang, Y., Jiang, X., Duong, T., Fan, C., Huang, C.-C., & Kain, S. R. (1998). Generation of Destabilized Green Fluorescent Protein as a Transcription Reporter. *Journal of Biological Chemistry*, *273*(52), 34970-34975. https://doi.org/10.1074/jbc.273.52.34970

Liu, X., Ramirez, S., Pang, P. T., Puryear, C. B., Govindarajan, A., Deisseroth, K., & Tonegawa, S. (2012). Optogenetic stimulation of a hippocampal engram activates fear memory recall. *Nature*, *484*(7394), 381-385. https://doi.org/10.1038/nature11028

Lovett-Barron, M., Kaifosh, P., Kheirbek, M. A., Danielson, N., Zaremba, J. D., Reardon, T. R., Turi, G. F., Hen, R., Zemelman, B. V., & Losonczy, A. (2014). Dendritic Inhibition in the Hippocampus Supports Fear Learning. *Science*, *343*(6173), 857-863. https://doi.org/10.1126/science.1247485

Marchal, C., & Mulle, C. (2004). Postnatal maturation of mossy fibre excitatory transmission in mouse CA3 pyramidal cells : A potential role for kainate receptors. *The Journal of Physiology*, *561*(1), 27-37. https://doi.org/10.1113/jphysiol.2004.069922

Marneffe, C., Moreira-de-Sá, A., Lecomte, S., Erhardt, A., & Mulle, C. (2024). Short term plasticity at hippocampal mossy fiber synapses. *Neuroscience*, S0306452224004974. https://doi.org/10.1016/j.neuroscience.2024.09.044

Maruo, T., Mandai, K., Takai, Y., & Mori, M. (2016). Activity-dependent alteration of the morphology of a hippocampal giant synapse. *Molecular and Cellular Neuroscience*, *71*, 25-33. https://doi.org/10.1016/j.mcn.2015.12.005

Matz, M. V., Fradkov, A. F., Labas, Y. A., Savitsky, A. P., Zaraisky, A. G., Markelov, M. L., & Lukyanov, S. A. (1999). Fluorescent proteins from nonbioluminescent Anthozoa species. *Nature Biotechnology*, *17*(10), 969-973. https://doi.org/10.1038/13657

McNaughtonis, L. (1987). *Hippocampalsynapticenhancementand informationstorage withina disMbutedmemorysystem*. *10*(10).

Milczarek, M. M., Vann, S. D., & Sengpiel, F. (2018). Spatial Memory Engram in the Mouse Retrosplenial Cortex. *Current Biology*, *28*(12), 1975-1980.e6. https://doi.org/10.1016/j.cub.2018.05.002

Mocle, A. J., Ramsaran, A. I., Jacob, A. D., Rashid, A. J., Luchetti, A., Tran, L. M., Richards, B. A., Frankland, P. W., & Josselyn, S. A. (2024). Excitability mediates allocation of pre-configured ensembles to a hippocampal engram supporting contextual conditioned threat in mice. *Neuron*, *112*(9), 1487-1497.e6.

https://doi.org/10.1016/j.neuron.2024.02.007

Nakamura, N. H., Flasbeck, V., Maingret, N., Kitsukawa, T., & Sauvage, M. M. (2013). Proximodistal Segregation of Nonspatial Information in CA3 : Preferential Recruitment of a Proximal CA3-Distal CA1 Network in Nonspatial Recognition Memory. *Journal of Neuroscience*, *33*(28), 11506-11514. https://doi.org/10.1523/JNEUROSCI.4480-12.2013

Nakazawa, K., Quirk, M. C., Chitwood, R. A., Watanabe, M., Yeckel, M. F., Sun, L. D., Kato, A., Carr, C. A., Johnston, D., Wilson, M. A., & Tonegawa, S. (2002). Requirement for Hippocampal CA3 NMDA Receptors in Associative Memory Recall. *Science*, *297*(5579), 211-218. https://doi.org/10.1126/science.1071795

Nakazawa, K., Sun, L. D., Quirk, M. C., Rondi-Reig, L., Wilson, M. A., & Tonegawa, S. (2003). Hippocampal CA3 NMDA Receptors Are Crucial for Memory Acquisition of One-Time Experience. *Neuron*, *38*(2), 305-315. https://doi.org/10.1016/S0896-6273(03)00165-X

Nakazawa, Y., Pevzner, A., Tanaka, K. Z., & Wiltgen, B. J. (2016). Memory retrieval along the proximodistal axis of CA1 : PROXIMODISTAL CA1. *Hippocampus*, *26*(9), 1140-1148. https://doi.org/10.1002/hipo.22596

Pernía-Andrade, A. J., Goswami, S. P., Stickler, Y., Fröbe, U., Schlögl, A., & Jonas, P. (2012). A Deconvolution-Based Method with High Sensitivity and Temporal Resolution for Detection of Spontaneous Synaptic Currents In Vitro and In Vivo. *Biophysical Journal*, *103*(7), 1429-1439. https://doi.org/10.1016/j.bpj.2012.08.039

Pignatelli, M., Ryan, T. J., Roy, D. S., Lovett, C., Smith, L. M., Muralidhar, S., & Tonegawa, S. (2019). Engram Cell Excitability State Determines the Efficacy of Memory Retrieval. *Neuron*, *101*(2), 274-284.e5. https://doi.org/10.1016/j.neuron.2018.11.029

Rebola, N., Carta, M., & Mulle, C. (2017). Operation and plasticity of hippocampal CA3 circuits : Implications for memory encoding. *Nature Reviews Neuroscience*, *18*(4), 208-220. https://doi.org/10.1038/nrn.2017.10

Reijmers, L. G., Perkins, B. L., Matsuo, N., & Mayford, M. (2007). Localization of a Stable Neural Correlate of Associative Memory. *Science*, *317*(5842), 1230-1233. https://doi.org/10.1126/science.1143839

Ruediger, S., Vittori, C., Bednarek, E., Genoud, C., Strata, P., Sacchetti, B., & Caroni, P. (2011). Learning-related feedforward inhibitory connectivity growth required for memory precision. *Nature*, *473*(7348), 514-518. https://doi.org/10.1038/nature09946

Ryan, T. J., Roy, D. S., Pignatelli, M., Arons, A., & Tonegawa, S. (2015). Engram cells retain memory under retrograde amnesia. *Science*, *348*(6238), 1007-1013. https://doi.org/10.1126/science.aaa5542

Sachidhanandam, S., Blanchet, C., Jeantet, Y., Cho, Y. H., & Mulle, C. (2009). Kainate Receptors Act as Conditional Amplifiers of Spike Transmission at Hippocampal Mossy Fiber Synapses. *The Journal of Neuroscience*, *29*(15), 5000-5008. https://doi.org/10.1523/JNEUROSCI.5807-08.2009

Sørensen, A. T., Cooper, Y. A., Baratta, M. V., Weng, F.-J., Zhang, Y., Ramamoorthi, K., Fropf, R., LaVerriere, E., Xue, J., Young, A., Schneider, C., Gøtzsche, C. R., Hemberg, M., Yin, J. C., Maier, S. F., & Lin, Y. (2016). A robust activity marking system for exploring active neuronal ensembles. *eLife*, *5*, e13918. https://doi.org/10.7554/eLife.13918

Sun, Q., Sotayo, A., Cazzulino, A. S., Snyder, A. M., Denny, C. A., & Siegelbaum, S. A. (2017). Proximodistal Heterogeneity of Hippocampal CA3 Pyramidal Neuron Intrinsic Properties, Connectivity, and Reactivation during Memory Recall. *Neuron*, *95*(3), 656-672.e3. https://doi.org/10.1016/j.neuron.2017.07.012

Sun, X., Bernstein, M. J., Meng, M., Rao, S., Sørensen, A. T., Yao, L., Zhang, X., Anikeeva, P. O., & Lin, Y. (2020). Functionally Distinct Neuronal Ensembles within the Memory Engram. *Cell*, *181*(2), 410-423.e17. https://doi.org/10.1016/j.cell.2020.02.055

Takeuchi, T., Duszkiewicz, A. J., & Morris, R. G. M. (2014). The synaptic plasticity and memory hypothesis : Encoding, storage and persistence. *Philosophical Transactions of the Royal Society B: Biological Sciences*, *369*(1633), 20130288. https://doi.org/10.1098/rstb.2013.0288

Thompson, L. T., Moyer, J. R., & Disterhoft, J. F. (1996). Transient changes in excitability of rabbit CA3 neurons with a time course appropriate to support memory consolidation. *Journal of Neurophysiology*, *76*(3), 1836-1849. https://doi.org/10.1152/jn.1996.76.3.1836

Tomé, D. F., Zhang, Y., Aida, T., Mosto, O., Lu, Y., Chen, M., Sadeh, S., Roy, D. S., & Clopath, C. (2024). Dynamic and selective engrams emerge with memory consolidation. *Nature Neuroscience*, *27*(3), 561-572. https://doi.org/10.1038/s41593-023-01551-w

Tonegawa, S., Liu, X., Ramirez, S., & Redondo, R. (2015). Memory Engram Cells Have Come of Age. *Neuron*, *87*(5), 918-931. https://doi.org/10.1016/j.neuron.2015.08.002

Torborg, C. L., Nakashiba, T., Tonegawa, S., & McBain, C. J. (2010). Control of CA3 Output by Feedforward Inhibition Despite Developmental Changes in the Excitation–Inhibition Balance. *The Journal of Neuroscience*, *30*(46), 15628-15637. https://doi.org/10.1523/JNEUROSCI.3099-10.2010

Tulving, E. (2002). Episodic Memory : From Mind to Brain. *Annual Review of Psychology*, *53*(1), 1-25. https://doi.org/10.1146/annurev.psych.53.100901.135114

Vandael, D., & Jonas, P. (2024). Structure, biophysics, and circuit function of a “giant” cortical presynaptic terminal. *Science*, *383*(6687), eadg6757. https://doi.org/10.1126/science.adg6757

Vetere, G., Tran, L. M., Moberg, S., Steadman, P. E., Restivo, L., Morrison, F. G., Ressler, K. J., Josselyn, S. A., & Frankland, P. W. (2019). Memory formation in the absence of experience. *Nature Neuroscience*, *22*(6), 933-940. https://doi.org/10.1038/s41593-019-0389-0

Weng, F.-J., Garcia, R. I., Lutzu, S., Alviña, K., Zhang, Y., Dushko, M., Ku, T., Zemoura, K., Rich, D., Garcia-Dominguez, D., Hung, M., Yelhekar, T. D., Sørensen, A. T., Xu, W., Chung, K., Castillo, P. E., & Lin, Y. (2018). Npas4 Is a Critical Regulator of Learning-Induced Plasticity at Mossy Fiber-CA3 Synapses during Contextual Memory Formation. *Neuron*, *97*(5), 1137-1152.e5. https://doi.org/10.1016/j.neuron.2018.01.026

Yap, E.-L., Pettit, N. L., Davis, C. P., Nagy, M. A., Harmin, D. A., Golden, E., Dagliyan, O., Lin, C., Rudolph, S., Sharma, N., Griffith, E. C., Harvey, C. D., & Greenberg, M. E. (2021). Bidirectional perisomatic inhibitory plasticity of a Fos neuronal network. *Nature*, *590*(7844), 115-121. https://doi.org/10.1038/s41586-020-3031-0

Yiu, A. P., Mercaldo, V., Yan, C., Richards, B., Rashid, A. J., Hsiang, H.-L. L., Pressey, J., Mahadevan, V.,

741 Tran, M. M., Kushner, S. A., Woodin, M. A., Frankland, P. W., & Josselyn, S. A. (2014). Neurons Are
742 Recruited to a Memory Trace Based on Relative Neuronal Excitability Immediately before Training.
743 *Neuron*, *83*(3), 722-735. https://doi.org/10.1016/j.neuron.2014.07.017

744 Zhang, W., & Linden, D. J. (2003). The other side of the engram : Experience-driven changes in neuronal
745 intrinsic excitability. *Nature Reviews Neuroscience*, *4*(11), 885-900. https://doi.org/10.1038/nrn1248

746 Zucca, S., Griguoli, M., Malézieux, M., Grosjean, N., Carta, M., & Mulle, C. (2017). Control of Spike
747 Transfer at Hippocampal Mossy Fiber Synapses *In Vivo* by $GABA_A$ and $GABA_B$ Receptor-Mediated
748 Inhibition. *The Journal of Neuroscience*, *37*(3), 587-598. https://doi.org/10.1523/JNEUROSCI.2057-
749 16.2016

750

751

752 **Figure Legends**

753 **Figure 1. Development of a novel viral tool to study early changes in the properties of CA3 engram**
754 **cells**. (**A**) Scheme representing the maturation of engram neurons during memory formation. Top panel:
755 during learning, a neuron receives numerous synaptic inputs, resulting in sequences of action potentials.
756 This activity triggers the rapid expression of immediate early genes (IEGs), marking the neuron as part of
757 an engram (yellow). As the engram matures (green), IEGs expression is not detectable anymore, yet the
758 neuron retains established engram properties. Bottom panel: expression function of IEG-based
759 construct to investigate and compare early and late engram properties. A construct with rapid offset
760 (yellow) best captures engrams shortly after learning, whereas a progressively expressing construct best
761 captures more mature engrams. (**B**) FLEN construct (c-Fos.ZsGreen1-DR) encapsulated in AAV2/9 vector.
762 Bottom panel: representative images showing ZsGreen1 fluorescence in c-Fos+ neurons (arrowhead)
763 and c-Fos- neurons (arrow). Scalebar = 50 µm. (**C**) Timeline of *in vitro* experiments to determine FLEN
764 expression and offset time course. After infection (DIV3) and activation (DIV11), samples are washed
765 with a blocking medium and images are acquired at different intervals (downward arrows). (**D**)
766 Percentage of ZsGreen+ vs. all transduced neurons (mCherry+ cells) at the different intervals following
767 activation. (**E**) Representative images of activated cultured neurons at 1, 2, 3, 4.5 and 6 hours after
768 activation. Scalebar = 100 µm.

769 **Figure 2. *In vivo* FLEN labeling and decay time course following a salient experience.** (**A**) FLEN and an
770 infection marker viral vectors are injected bilaterally into CA3. Mice undergo contextual fear
771 conditioning (CFC), and sections are collected (downward arrows) 1.5, 3, 4.5, 6 and 12 hours following
772 CFC. As a control, sections are obtained from mice left undisturbed in their home cage (HC). (**B**) Left:
773 one-time CFC experiment scheme. Mice explore an arena for 5 minutes, 3 foot-shocks are given at 180,
774 210 and 270 seconds after the start of the test (red line). Top-right: paired comparison of the
775 percentage of time mice spent freezing during training and when replaced in the conditioning arena 1
776 hour after CFC. Bottom-right: comparison of the percentage of time mice spent freezing during training,
777 when placed in a different neutral environment and 24 hours after CFC. These experiments show that
778 the CA3-dependent shock-context association is rapidly learned (within 1 hour), is highly environment-
779 selective and it is retained for 24 hours. (**C**) Representative images of CA3 neurons expressing the
780 infection marker (mCherry+, indicated by arrow) and neurons expressing both the infection marker and
781 FLEN (ZsGreen1+/mCherry+, indicated by arrowhead). The latter are considered FLEN+ neurons.
782 Scalebar = 50 µm. (**D**) Percentage of ZsGreen+ CA3 neurons over the total number of mCherry+ neurons

783 at different intervals following activation. (**E**) Representative sections of CFC-trained mice compared to
784 HC untrained mice at different intervals following CFC. Dashed lines outline the dentate gyrus (DG)
785 cellular layer, while the dashed segment indicates the separation between CA3 and CA2. Scale bar = 100
786 µm. (**F**) Left panel: Schematic representation of neuronal position along the proximodistal axis analysis
787 of CA3. The CA3 pyramidal layer was straightened and the x position of FLEN+ cells was normalized on a
788 0 (closer to DG) to 1 (closer to CA2) scale. Right panel: comparison of normalized proximodistal
789 frequency distribution of CA3 FLEN+ cells placement in HC mice (gray) and 3 hours post-CFC mice
790 (yellow). Bold lines represent the median of the respective distributions. HC median is displayed in the
791 CFC plot to highlight distribution difference.

792 **Figure 3. Electrophysiological analysis of intrinsic properties of CA3 engram neurons**. (**A**) Experimental
793 outline: mice were injected with either FLEN or RAM construct, subjected to CFC and then sacrificed at
794 either 3- or 24-hours post-conditioning to collect acute hippocampal slices. Right: representative images
795 of FLEN+ and RAM+ cells targeted for patch clamp recordings, with neighboring control FLEN- or RAM-
796 neurons. Scale bar = 20 µm. (**B**) Membrane potential response. Left panel: representative membrane
797 potential trace in response to incremental injected current in control cells (gray) and engram cells
798 (yellow for FLEN and green for RAM). Right panel: graphs of input resistance for comparison between
799 engram cells and their corresponding control cells. (**C**) Action potential firing pattern. Left panel: sample
800 traces of long (1 second) above-rheobase current step to analyze the pattern of action potential firing
801 current in control cells (gray) and engram cells (yellow and green). Right panel: average spike frequency
802 graphs. (**D**) Cumulative spike frequency curve over the 1 second current step shown in (C) showing a
803 similar distribution between FLEN+ and FLEN – neurons (top), and a more sustained firing of RAM+
804 compared to their RAM- neurons (bottom).

805 **Figure 4. Analysis of EPSCs and IPSCs in CA3 engram neurons** (**A**) Sample traces and cumulative
806 distributions of sEPSCs recorded from CA3 engram neurons (FLEN in yellow, RAM in green). Top panels:
807 comparison between $FLEN^+$ and $FLEN^-$ neurons reports no difference in mean sEPSC amplitude
808 cumulative distribution but a higher event frequency in $FLEN^+$ neurons, as seen in the inter-event
809 interval (IEI) cumulative distribution. Inset displays the comparison of the average frequency (Hz) of such
810 events. Bottom panels: RAM^+ vs RAM^- neurons show a similar pattern characterized by no change in
811 amplitude and increased frequency in RAM^+ neurons. (**B**) Same analysis as in (A), for miniature EPSCs
812 (mEPSCs). The inset in the amplitude plot shows the fraction of mEPSCs exceeding 40 pA, indicative of

giant mossy fiber events. (**C**) As (A) and (B), for miniature IPSCs (mIPSCs), comparing frequency and amplitude in FLEN+ vs FLEN- and RAM+ vs, RAM- neurons.

Figure 5. Properties of Mf-CA3 synapses in CA3 engram neurons (**A**) Schematic representation of Mf-CA3 EPSCs and feedfoward inhibition recordings. (**B**) Left panel: representative traces showing EPSC amplitude in FLEN- (gray) and FLEN+ (yellow) cells following low frequency stimulation (0.1 Hz) and corresponding increase evoked with a higher stimulation frequency (1 Hz), due to a presynaptic form of synaptic plasticity characteristics of Mf-CA3 synapses (frequency facilitation). Center panel: amplitude plot for FLEN- and FLEN+ stimulated at 0.1 Hz and 1 Hz. Right panel: frequency facilitation ratio plot shows no difference between FLEN- and FLEN+ neurons. (**C**) Left panel: representative traces showing Mf-driven IPSCs (feedforward inhibition) and EPSCs (direct excitatory activity) recorded in individual FLEN- (gray) and FLEN+ (yellow) neurons. Center panel: amplitude plot of EPSCs and IPSCs for FLEN- and FLEN+ neurons. Right panel: graph showing excitation-to-inhibition ratio, comparing FLEN- and FLEN+ neurons.

Figure 1

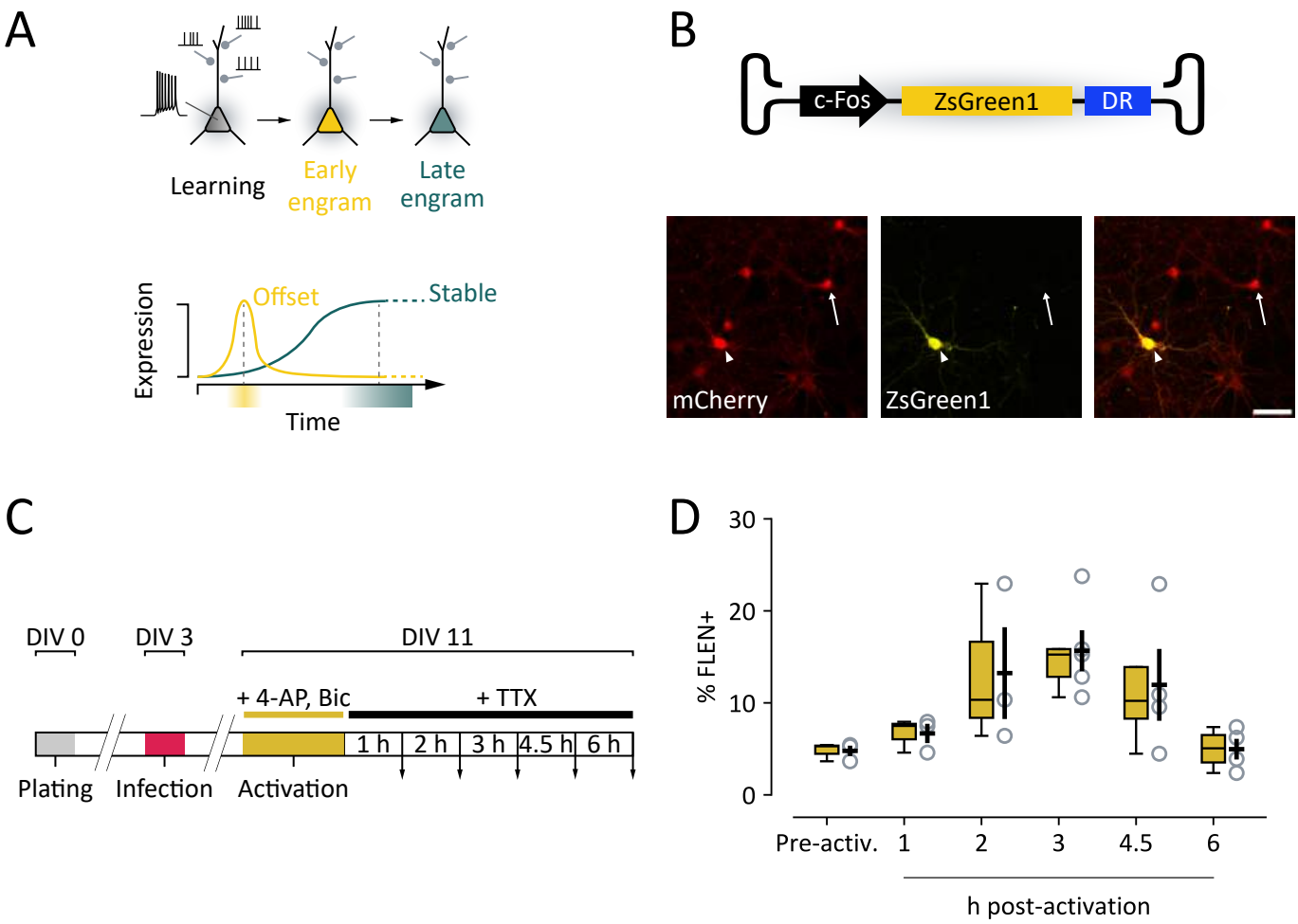
A
Learning
Early engram
Late engram
Expression
Offset
Stable
Time
B
c-Fos
ZsGreen1
DR
mCherry
ZsGreen1
C
DIV 0
DIV 3
DIV 11
+ 4-AP, Bic
+ TTX
1 h
2 h
3 h
4.5 h
6 h
Plating
Infection
Activation
D
% FLEN+
30
20
10
0
Pre-activ.
1
2
3
4.5
6
h post-activation

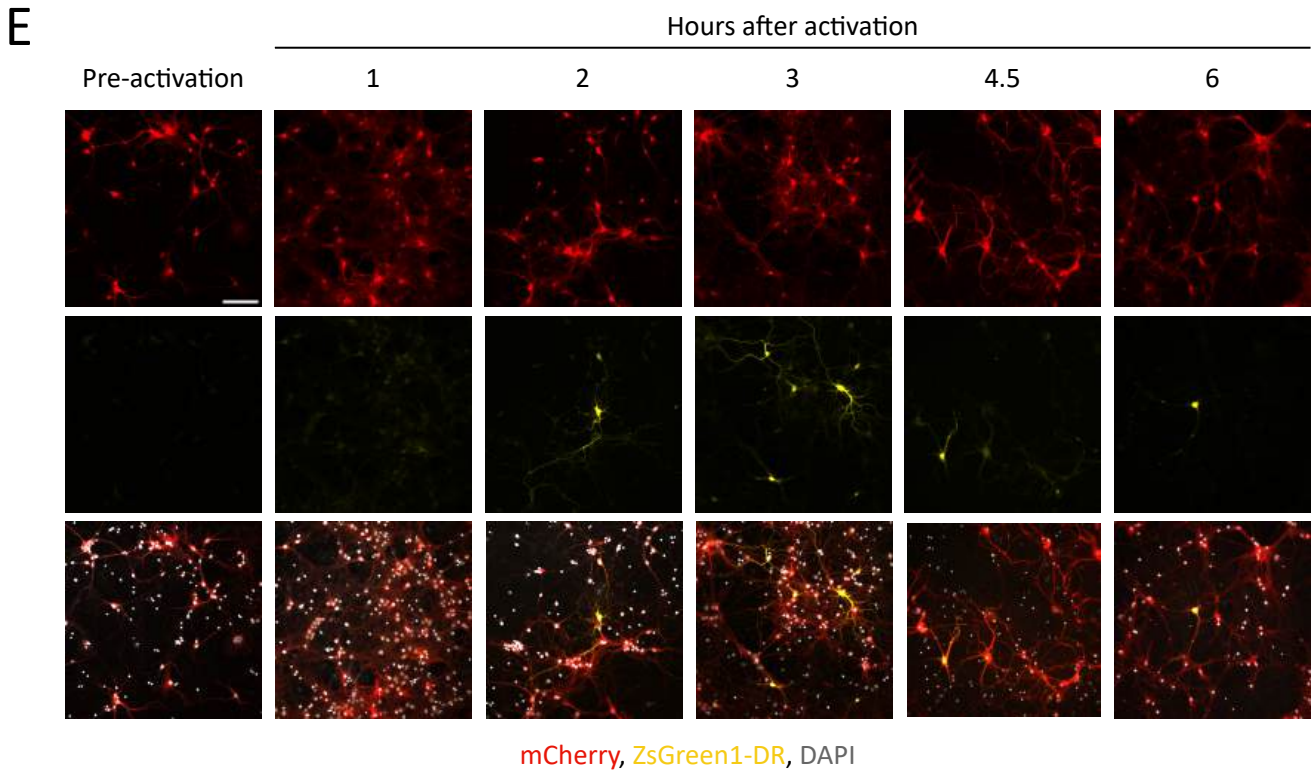
E
Hours after activation
Pre-activation
1
2
3
4.5
6
mCherry, ZsGreen1-DR, DAPI

Figure 2

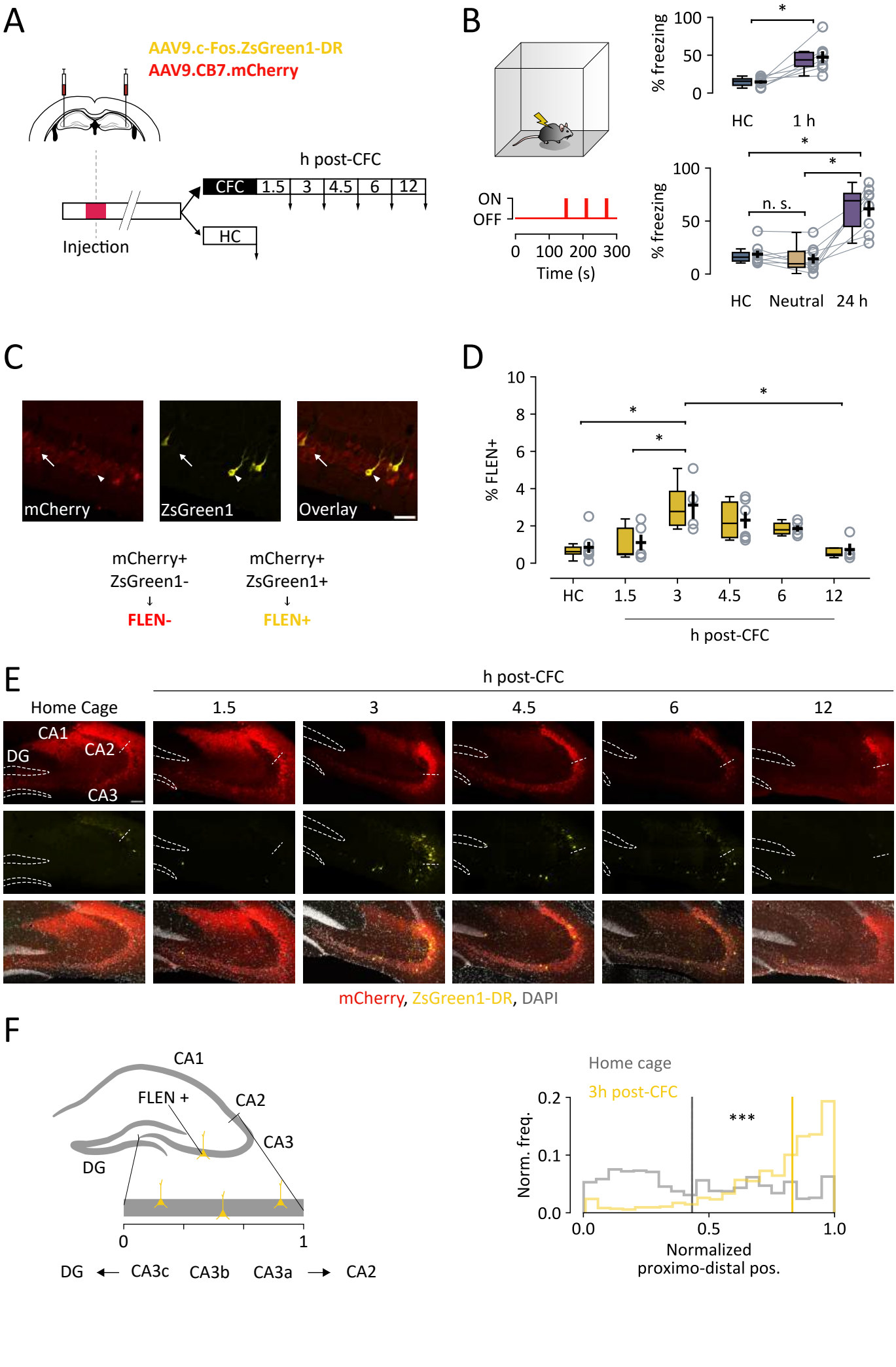
A
AAV9.c-Fos.ZsGreen1-DR
AAV9.CB7.mCherry
h post-CFC
CFC
1.5
3
4.5
6
12
HC
Injection
B
ON
OFF
0
100
200
300
Time (s)
% freezing
100
50
0
*
HC
1 h
*
*
n. s.
HC
Neutral
24 h
C
mCherry
ZsGreen1
Overlay
mCherry+
ZsGreen1-
FLEN-
mCherry+
ZsGreen1+
FLEN+
D
% FLEN+
10
8
6
4
2
0
HC
1.5
3
4.5
6
12
h post-CFC
E
h post-CFC
Home Cage
1.5
3
4.5
6
12
CA1
CA2
DG
CA3
mCherry, ZsGreen1-DR, DAPI
F
CA1
FLEN +
CA2
CA3
DG
0
1
DG ← CA3c CA3b CA3a → CA2
Home cage
3h post-CFC
Norm. freq.
0.2
0.1
0.0
***
0.0
0.5
1.0
Normalized
proximo-distal pos.

Figure 3

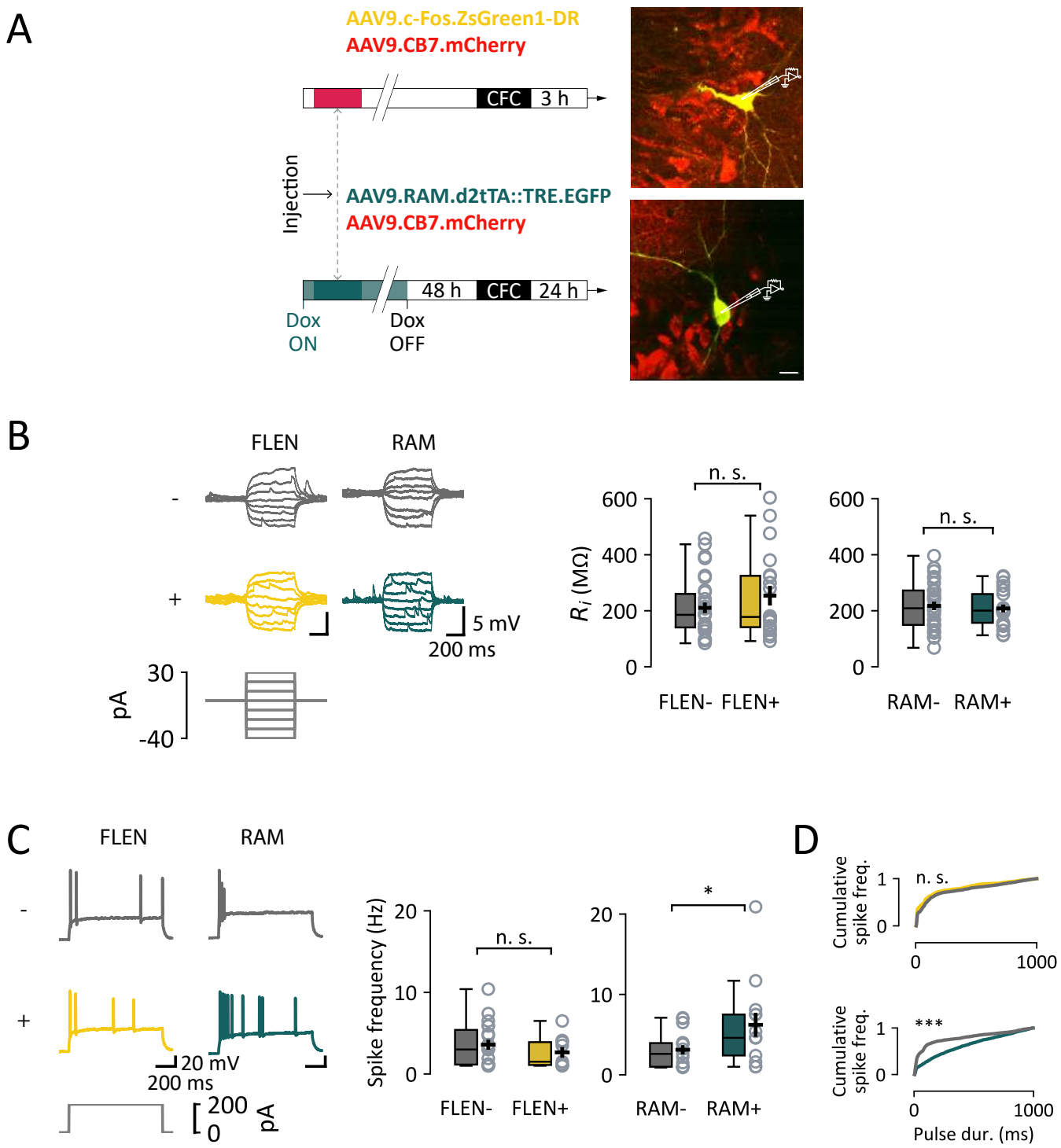
A
AAV9.c-Fos.ZsGreen1-DR
AAV9.CB7.mCherry
CFC
3 h
Injection
AAV9.RAM.d2tTA::TRE.EGFP
AAV9.CB7.mCherry
48 h
CFC
24 h
Dox ON
Dox OFF
B
FLEN
RAM
-
+
5 mV
200 ms
30
pA
-40
n. s.
600
400
200
0
R_i (MΩ)
FLEN-
FLEN+
RAM-
RAM+
C
FLEN
RAM
20 mV
200 ms
200
0
pA
Spike frequency (Hz)
20
10
0
n. s.
*
D
Cumulative spike freq.
1
0
n. s.
***
0
1000
Pulse dur. (ms)

Figure 4

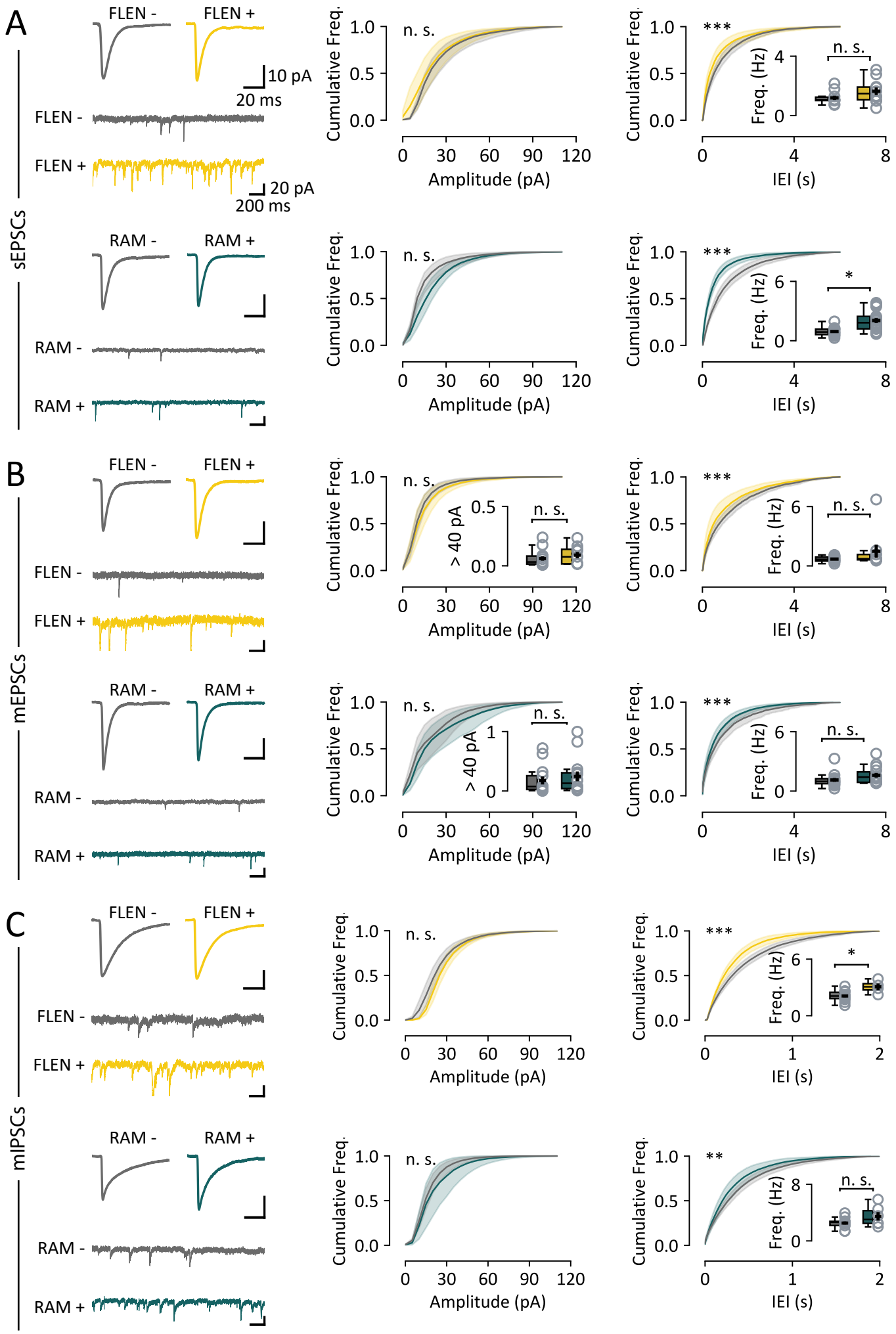
A
sEPSCs
FLEN -
FLEN +
10 pA
20 ms
20 pA
200 ms
RAM -
RAM +
B
mEPSCs
C
mIPSCs
Cumulative Freq.
n. s.
Amplitude (pA)
IEI (s)
Freq. (Hz)
> 40 pA
***
**
*

Figure 5

A

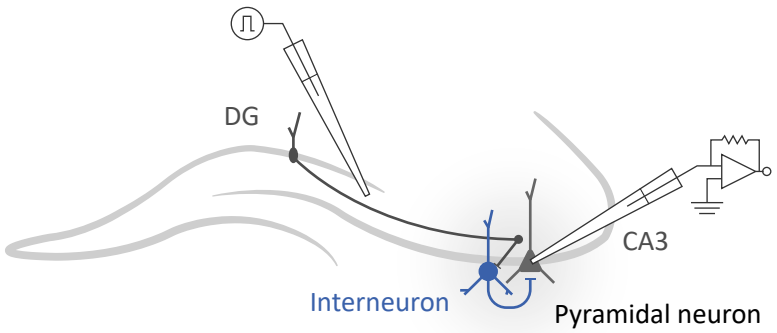
DG
CA3
Interneuron
Pyramidal neuron

B

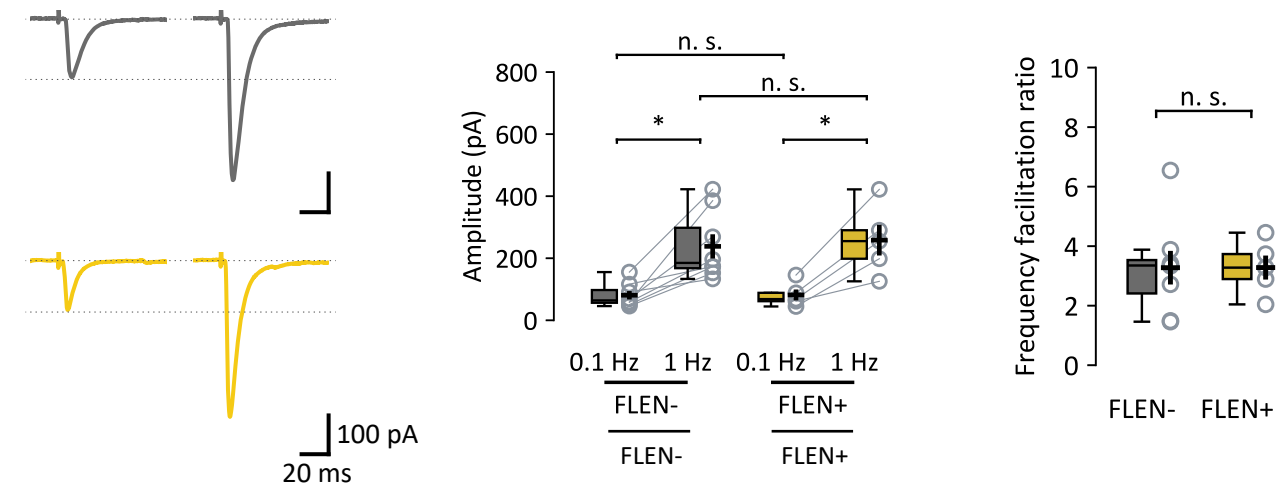
100 pA
20 ms
Amplitude (pA)
800
600
400
200
0
n. s.
n. s.
*
*
0.1 Hz
1 Hz
0.1 Hz
1 Hz
FLEN-
FLEN-
FLEN+
FLEN+
Frequency facilitation ratio
10
8
6
4
2
0
n. s.
FLEN-
FLEN+

C

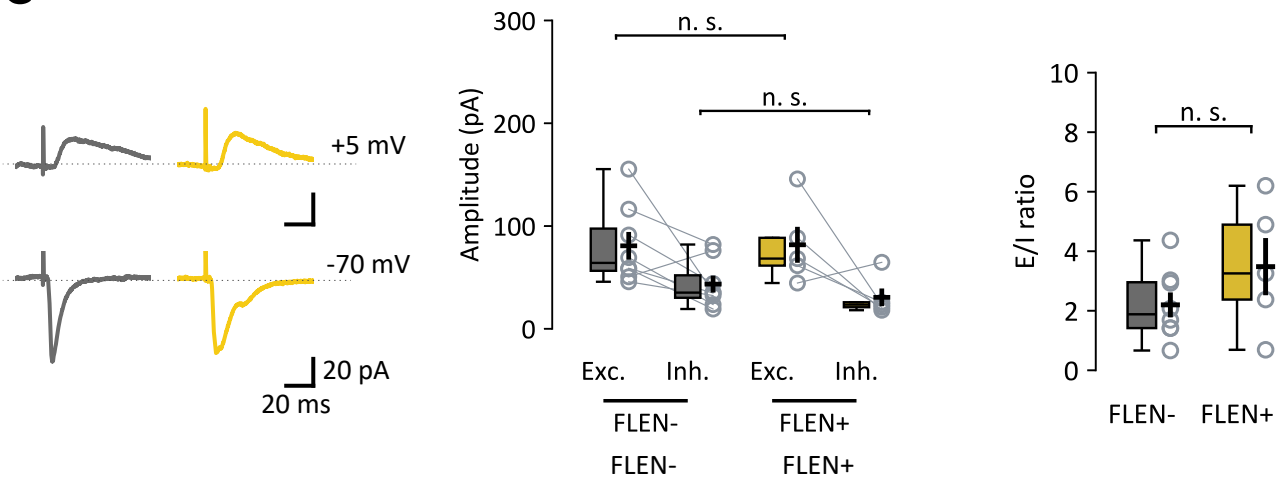
+5 mV
-70 mV
20 pA
20 ms
Amplitude (pA)
300
200
100
0
n. s.
n. s.
Exc.
Inh.
Exc.
Inh.
FLEN-
FLEN-
FLEN+
FLEN+
E/I ratio
10
8
6
4
2
0
n. s.
FLEN-
FLEN+